THESIS FOR THE DEGREE OF DOCTOR OF PHILOSOPHY

The effect of workpiece material and its microstructure on tool wear in metal cutting

Philipp Hoier

Department of Industrial and Materials Science

CHALMERS UNIVERSITY OF TECHNOLOGY

Gothenburg, Sweden 2019

The effect of workpiece material and its microstructure on tool wear in metal cutting

PHILIPP HOIER
ISBN 978-91-7905-141-9

Doktorsavhandlingar vid Chalmers tekniska högskola
Ny serie nr 4608
ISSN 0346-718X

Department of Industrial and Materials Science
Chalmers University of Technology
SE-412 96 Gothenburg
Sweden
Telephone + 46 (0)31-772 1000

Chalmers Reproservice

Gothenburg, Sweden 2019

The effect of workpiece material and its microstructure on tool wear in metal cutting

PHILIPP HOIER

Department of Industrial and Materials Science

Chalmers University of Technology

Abstract

The aim of the present work is to promote the basic understanding of how the workpiece material and its microstructure affect the tool wear during metal cutting. To isolate the effect of the workpiece material, the tool material (uncoated cemented carbide) was kept constant while the workpiece was varied. The studied workpiece materials were a tool steel, two superalloys, a case-hardening steel, and two workpieces of an austenitic stainless steel obtained from different suppliers. After controlled turning tests, the workpiece microstructures and the resulting tool wear was studied, primarily by scanning electron microscopy together with energy-dispersive X-ray spectroscopy and the electron backscatter diffraction technique.

The results show that the thermo-mechanical and microstructural properties of the different workpieces result in distinct microscopic features on the worn tool surfaces. The responsible wear mechanisms were identified by assessing the chemical and physical properties of the microstructural constituents in the workpieces. Due to its large amounts of carbides, machining the tool steel was primarily associated with abrasive tool wear. The corresponding wear features on the tungsten carbide grains were dominated by grooves, micro-fragmentation, and plastic deformation. Similarly, abrasion played a major role when machining the superalloys. Differences in the amount of carbides and inclusions triggered varying degrees of abrasion which affected the overall flank wear when cutting the two investigated superalloys. Flank wear resulting from machining the case-hardening steel is suggested to be due to dissolution combined with mild abrasion. In contrast, the stainless steel workpieces did not contain significant amounts of hard phases which led to mainly dissolution-induced flank wear. The worn tool surfaces were characterized by smooth tungsten carbide grains without micro-fragmentation or plastic deformation. For the two stainless steel workpieces, the non-metallic inclusions and their ability to form stable layers on the tool surfaces controlled the overall flank wear. If present, a stable inclusion layer provides protection of the underlying tool material against dissolution. Knowledge of the active tool wear mechanisms and their underlying reasons can be used as input for physics-based wear modelling approaches and allows to identify the role of microstructural variations in workpieces. In that way, the cutting process can be optimized to become more reliable, efficient, and sustainable.

Keywords: Machining; Cutting tool; Wear; Cemented carbide; Steel; Superalloy; Scanning electron microscopy.

Preface

The present thesis is based on work carried out at the Department of Industrial and Materials Science (Department of Materials and Manufacturing Technology until May 2017) at Chalmers University of Technology in the time between September 2014 and July 2019.

The work was supervised by Prof. Uta Klement together with Prof. Peter Krajnik and Prof. Tomas Beno (University West, Trollhättan). Funding has been received by Västra Götalandsregionen within the "PROSAM" project. The work was furthermore linked to the Area of Advance - Production and the Chalmers Centre for Metal Cutting Research "MCR" as well as to the project "WEAR-FRAME", funded by "Metallic Materials" -a joint venture of Vinnova, Formas and the Swedish Energy Agency.

The thesis consists of an introductory part followed by the appended papers listed below:

Paper I: Characterization of abrasion- and dissolution-induced tool wear in machining
P. Hoier, A. Malakizadi, U. Klement, P. Krajnik
Wear, Volumes 426-427, Pages 1548-1562, 2019.

Paper II: Study of flank wear topography and surface-deformation of cemented carbide tools after turning Alloy 718
P. Hoier, A. Malakizadi, P. Krajnik, U. Klement
Procedia CIRP, Volume 77, Pages 537-540, 2018.

Paper III: Microstructural characteristics of Alloy 718 and Waspaloy and their influence on flank wear during turning
P. Hoier, A. Malakizadi, P. Stuppa, S. Cedergren, U. Klement
Wear, Volumes 400-401, Pages 184-193, 2018.

Paper IV: Tool wear by dissolution during machining of Alloy 718 and Waspaloy: A comparative study using diffusion couples
P. Hoier, K.B. Surreddi, U. Klement
Submitted for publication

Paper V: A critical assessment of tool wear mechanisms when machining alloys with distinctive thermo-mechanical and microstructural properties
A. Malakizadi, P. Hoier, U. Klement, P. Krajnik
Manuscript

Paper VI: Microstructural variations in 316L austenitic stainless steel and their influence on tool wear in machining
P. Hoier, A. Malakizadi, S. Friebe, U. Klement, P. Krajnik
Wear, Volumes 428-429, Pages 315-327, 2019.

Contribution to the appended papers

Paper I: The author did the major part of microscopy on the workpieces and tools and supported the tool life tests. Dr. Amir Malakizadi performed the solubility calculations and the majority of the tool life tests. The results were analyzed and discussed with all co-authors. The author wrote the first draft of the paper.

Paper II: The author did all electron microscopy work and performed parts of the turning tests. The results were analyzed and discussed with all co-authors. The author wrote the first draft of the paper.

Paper III: The author did all microscopy on the workpieces and tools and executed parts of the tool life tests. The results were analyzed and discussed with all co-authors. The author wrote the first draft of the paper.

Paper IV: The author performed all scanning electron microscopy work. The results were analyzed and discussed with all co-authors. The author wrote the first draft of the paper.

Paper V: The author did the majority of microscopy work on the worn tools and the workpieces and executed parts of the turning tests. The cutting simulations were done by Dr. Amir Malakizadi. The author contributed to analysis and interpretation of the obtained results and writing of the manuscript.

Paper VI: The author did the majority of characterization of the workpieces and tools and supported the turning tests. The solubility calculations and the majority of the turning tests were performed by Dr. Amir Malakizadi. The results were analyzed and discussed with all co-authors. The author wrote the first draft of the paper.

Papers not appended to the thesis

- Effects of high-pressure cooling in the flank and rake faces of WC tool on the tool wear mechanism and process conditions in turning of alloy 718
  N.T. Alagan, P. Hoier, P. Zeman, U. Klement, T. Beno, A. Wretland
  Wear, 2019.
- Investigation of micro-textured cutting tools used for face turning of alloy 718 with high-pressure cooling
  N.T. Alagan, P. Zeman, P. Hoier, T. Beno, U. Klement
  Journal of Manufacturing Processes, Volume 37, Pages 606-616, 2019.
- Influence of surface features for increased heat dissipation on tool wear
  N.T. Alagan, T. Beno, P. Hoier, U. Klement, A. Wretland
  Materials, Volume 11, Issue 5, 2018.
- Flank wear characteristics of WC-Co tools when turning Alloy 718 with high-pressure coolant supply
  P. Hoier, U. Klement, N.T. Alagan, T. Beno, A. Wretland
  Journal of Manufacturing Processes, Volume 30, Pages 116-123, 2017.
- Characterization of tool wear when machining alloy 718 with high-pressure cooling using conventional and surface-modified WC–Co tools
  P. Hoier, U. Klement, N.T. Alagan, T. Beno, A. Wretland
  Journal of Superhard Materials, Volume 39, Issue 3, Pages 178-185, 2017.

Table of Contents

1 Introduction

Metal cutting operations play a key role during the manufacture of nearly every metallic component used in engineering applications [1], [2]. The important role of metal cutting operations in the production of components is demonstrated in Fig. 1. As illustrated, large fractions of the overall costs of typical powertrain or aircraft-engine components can be attributed to machining, during which significant volumes of material are often removed. Furthermore, the produced component's form, accuracy and surface integrity are directly influenced by machining [3] and have to be met for the component to function properly.

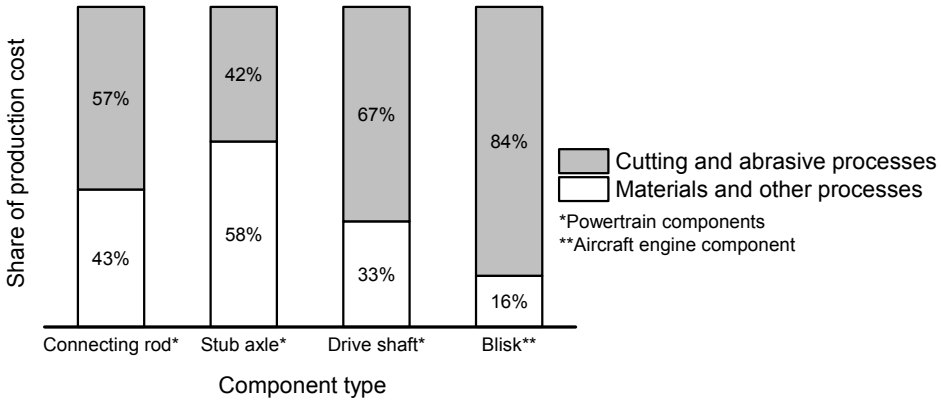

Fig. 1: Examples of manufacturing cost of some engineered components. Adapted from [2], [4].

In order to achieve a high level of productivity in a production line, it is important to have fast, robust and reliable machining processes. One source of process disruptions is due to wear of the cutting tools. During metal cutting, the employed cutting tools inevitably undergo gradual wear. Geometrical changes of the tools due to wear negatively affect several process characteristics. For example, high cutting forces and temperatures are directly related to excessive tool wear, resulting in poor geometrical accuracy and surface integrity of the machined component. An example of surface damage due to uncontrolled tool wear can be seen in Fig. 2. Since such damage has a negative effect on the component's performance (e.g. fatigue life), damaged components need to be repaired or scrapped which is undesirable from economical and environmental viewpoints. Furthermore, if the damage remains undetected during inspection at time of manufacture, premature failure of components can have serious consequences, especially in case of aircraft engine components [5].

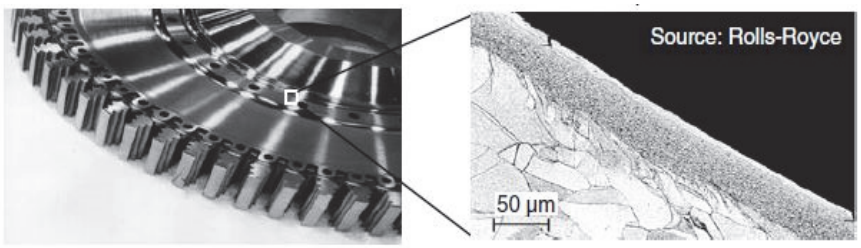

Fig. 2: Unfavorable surface integrity caused by drilling with a worn tool. The shown component is a turbine disk made from Alloy 718 [6]. *Figure reproduced with permission of Springer Nature*[1].

[1]Reprinted by permission from Springer Nature: Springer, Berlin, Heidelberg, Manufacturing Processes 1 by Fritz Klocke, Springer-Verlag Berlin Heidelberg 2011

In order to avoid surface damage and to meet component-design requirements, cutting tools need to be replaced before a critical amount of tool wear has been reached. Timely tool changes require steady and well understood tool wear rates for the respective tool/workpiece combination and employed set of cutting parameters [6].

In order to estimate tool life for certain tool/workpiece materials and cutting parameters, empirical tool life relations such as Taylor's tool life equation [7] are commonly used in the industry. However, despite the use of tool life relations, inconsistent tool wear responses are often encountered in production lines even when machining the same material/alloy. Such problems can arise when the input materials exhibit metallurgical variations, e.g. in large forgings or in materials from different suppliers with different processing histories prior to machining. To avoid or limit these effects, it is important to fundamentally understand the influence of the workpiece material and microstructure on the tool wear. Only then, the respective tool wear response can be estimated more precisely and countermeasures can be taken by for example adjusting the intervals of tool changes or by changing the composition or processing of the input material in order to get more favorable machining results.

In practice, however, it can be complicated to pin-point the exact microstructural aspect which is responsible for the inconsistent tool life response during machining. This is because many alloys feature complex microstructures with microstructural variations spanning across different length scales (mm to sub μm-scale). Furthermore, the influence of workpiece-constituents on the tool wear is complex and not well understood because a number of tool wear mechanisms are usually active simultaneously (e.g. abrasion, adhesion, dissolution). It is this overlap and the dynamics of the mechanisms which makes a systematic study and identification of the active tool wear mechanisms as well as of the underlying effect of the workpiece properties and microstructure challenging.

1.1 Objective and research questions

The overarching objective of the thesis is to advance the fundamental understanding of the effect of the workpiece material and its microstructure on the tool wear during metal cutting.

The objective of the work can be described by the following research questions (RQ):

- RQ1: What are the characteristic features on the worn tool surface resulting from machining the respective workpiece material?
- RQ2: What are the dominant wear mechanisms leading to the characteristic tool wear features during machining?
- RQ3: How are variations in the workpiece microstructure affecting the active wear mechanisms and the resulting overall tool wear?

1.2 Research approach

The complexity of tribology and tool wear in metal cutting is partly due to the fact that besides workpiece characteristics (e.g. composition, microstructure, mechanical properties), a number of additional interrelated factors also influence the thermo-mechanical loads and the resulting tool wear mechanisms. These factors include cooling and lubrication methods, the tool geometry, and the tool materials. In fact, a major part of published work in the field of metal cutting tool wear focusses on optimizing tool life by means of the aforementioned aspects, e.g. by changing the tool material, by applying advanced coatings [8] or by employing different lubrication methods [9], [10].

In order to narrow the research focus and to limit these effects, the research approach was to keep the cutting tool material constant and instead vary the workpieces in order to focus on the influence

of the machined material on the tool wear. This approach of "material-on-process" is not common in metal cutting research, as the research focus is typically the opposite, i.e. "process-on-material".

The chosen tool material was cemented tungsten carbide, used in the majority of machining operations. The bulk of the tests was done using uncoated cutting tools in order to limit the effect of coatings and to reduce the complexity of wear characterization. Only for two of the investigated workpieces some complementary tests were done using coated cutting tools (Paper I). In accordance with the research approach of a constant tool material for all workpieces, the results on the coated tools are therefore not discussed in detail within this thesis.

With the tool material being constant, several workpieces with varying properties and microstructures were machined as part of this work and the resulting tool wear was studied systematically. The focus of the wear characterization has been laid on the wear occurring on the clearance of the cutting tools, i.e. flank wear. The schematic in Fig. 3 provides an overview of the workpiece materials and how the formulated research questions (section 1.1) are taken up in the research approach and respective publications. The publications can be divided into studies addressing mainly:

- Flank wear mechanisms associated with machining the different types of materials (e.g. Paper I and Paper II). These studies mainly address RQ1 and RQ2.

- Identification of differences in workpiece microstructure and their influence on flank wear. These studies concern variations of flank wear when machining different alloys of the same material type (e.g. Alloy 718 and Waspaloy in Paper III) or workpieces of the same alloy (batch-to-batch variations in 316L, Paper VI). These studies are mainly addressing RQ3.

Generally, the approach in this work was to combine controlled machining tests with dedicated material characterization of both the workpieces and the worn tool surfaces (focused on the flank wear). In that way, it was possible to connect microstructural aspects (e.g. type and amount of carbides or inclusions) to the resulting wear characteristics and underlying tool wear mechanisms.

The aim of Paper I was to obtain primarily abrasive wear and wear by dissolution and thereby provide experimental evidence of these mechanisms. The information was used to assess the relative contributions of these mechanisms to the tool wear when machining other materials. Papers II, III, and IV were concerned with machining of heat-resistant superalloys for aerospace applications. The emphasis was to elucidate the difference in flank wear responses when machining two alloys, Alloy 718 and Waspaloy. In Paper V, the approach was extended and a case-hardening steel was included. In Paper VI, batch-to-batch material variations in a stainless steel and their influence on tool wear were in focus.

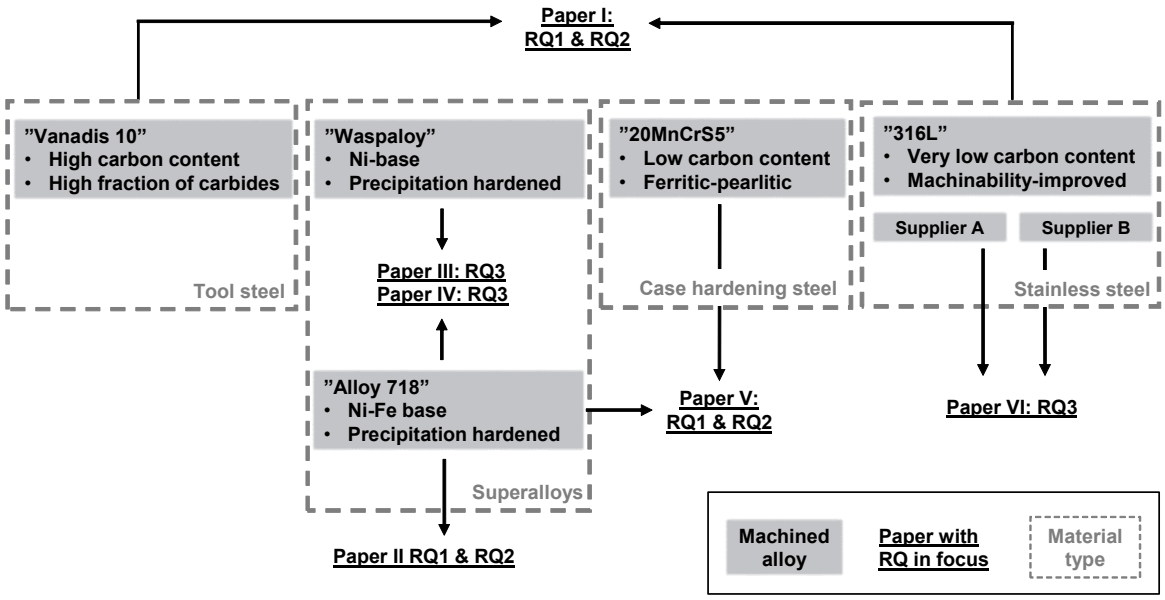

Fig. 3: Schematic of the research approach and case-studies with the investigated workpieces, their interconnection and the corresponding research questions (RQs) of interest.

1.3 Limitations

The microscopic examination of worn tools was conducted across different length scales and included many aspects (wear topography, surface deformation, composition of adhered layers etc.). The analysis was therefore limited to a selection of cutting tools and was not conducted for each replica of the tests. Furthermore, the wear characteristics of the tool's binder-phase was not studied in detail. Instead, characterization of the worn tools was performed on its main constituent tungsten carbide on the flank wear land.

As part of the research approach (section 1.2), uncoated cemented tungsten carbide inserts were used to focus on the influence of the workpiece material on the tool wear. This tool material is one of the most commonly applied materials in tools for many machining operations. However, uncoated tools are not the first choice for machining of some of the investigated workpiece materials. The comparably simple tool material without coatings was chosen in order to reduce the complexity of the analysis of the wear topographies and adhered layers and to correctly identify the active wear mechanisms during cutting. Moreover, even for coated inserts, the wear of the cemented carbide substrate becomes relevant since progressing tool wear usually results in the local loss of the coating which exposes the underlying tool substrate.

2 Metal cutting

In metal cutting operations (also referred to as machining), material is mechanically removed from a workpiece in form of chips [6] to produce a desired workpiece surface. There is a large variety of metal cutting operations which can be categorized as processes using geometrically defined cutting edges (e.g. turning and milling) or geometrically undefined cutting edges (e.g. grinding) [11]. By combining different metal cutting operations, components of complex geometry can be manufactured. Within this work, the focus was on turning, which is a process utilizing tools with defined cutting edges used to produce rotationally-symmetric components.

2.1 Turning

In turning, the workpiece is clamped in a rotating chuck and a cutting tool is fed into the workpiece. Chip formation takes place due to the relative movement between the tool and the workpiece. Depending on whether the tool is fed in radial direction or longitudinal direction, turning operations can be termed as facing or longitudinal turning respectively [6]. The illustration in Fig. 4a shows a longitudinal turning operation where the tool is moving parallel to the axis of workpiece-rotation.

The illustration in Fig. 4a also shows the major process parameters. The relative speed between tool and workpiece at the point of contact is the cutting speed, v_c, which is usually expressed in m/min. The distance by which the tool is fed during every revolution of the workpiece is the feed rate, f, usually expressed in mm/rev. The thickness of the removed layer is the depth of cut, a_p, which is perpendicular to the feed direction and expressed in mm.

The force acting on the tool during machining can be measured using piezoelectric force sensors. It can be split up into three force components, shown in Fig. 4b. The main cutting force (F_c) acts on the rake face of the tool in the direction of the cutting speed. The force acting on the flank face and parallel to the feed direction is termed feed force (F_f). Finally, the passive force (F_p) is the force component that pushes the tool away from the workpiece, i.e. in radial direction in case of longitudinal turning.

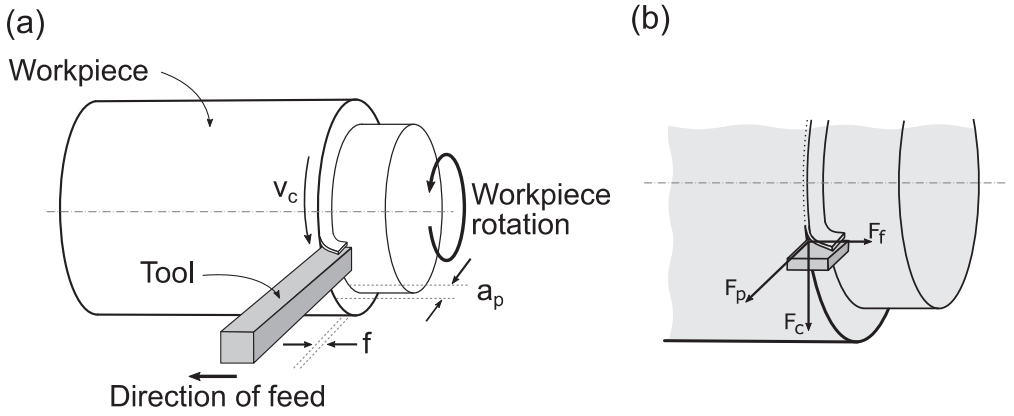

Fig. 4: (a) Illustration of a turning process where the tool is fed in longitudinal direction. Key process parameters cutting speed (v_c), feed rate (f), and depth of cut (a_p) are indicated. (b) Schematic showing the directions of the three force components, main cutting force (F_c), feed force (F_f), and passive force (F_p) acting on the tool during longitudinal turning. Image courtesy of Simon Isakson [12].

2.2 The cutting zone

A simplified, cross-sectional view of the contact zone between workpiece, tool, and generated chip is shown schematically in Fig. 5. Shearing of workpiece material and subsequent removal in form

of chips occurs due to the relative motion between the tool and the workpiece (indicated by cutting speed, v_c). As a result of shearing the workpiece material, almost all of the used mechanical work is converted into heat during cutting [6].

During cutting, severe plastic deformation of the workpiece material occurs at a high rate in the primary (1), secondary (2), and tertiary (3) shearing zones [6], see Fig. 5. Accurate determination of the respective strain and strain-rates in the cutting zone is very challenging and reported values are often based on simplified shear plane models [13]. However, strains of 100 to 700% and strain-rates of up to 10^6 s^{-1} have been reported together with high pressures (nearly 2 to 3 GPa) and temperatures exceeding 1000 °C [14].

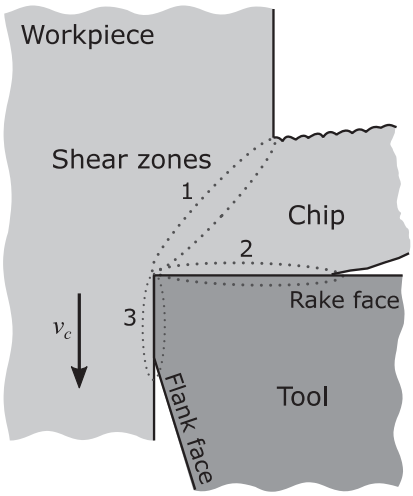

Fig. 5: Schematic of the cutting zone showing the process of chip formation in cross section: The three shear zones (1-3) are encircled and the direction of cutting speed (v_c) is indicated. The figure was adapted from [12].

3 Cutting tool materials and tool wear

The requirements on tool materials include high hardness to resist abrasive wear combined with sufficient toughness and compressive strength to resist fracture and plastic deformation. Furthermore, chemical stability and inertness to the machined workpiece is required. Among common cutting tool materials, cemented carbides are the most versatile material group [15]. As compared with e.g. super-hard materials like ceramics, cubic boron nitride, and diamond which suffer from comparably low toughness, cemented carbides have a unique combination of high bulk hardness and toughness within a comparably wide range [15].

This section is devoted to introducing cemented carbides for cutting tool applications as well as the most common tool wear forms and mechanisms in metal cutting.

3.1 Cemented carbides

Cemented carbide is a composite material which is produced by powder metallurgy using liquid phase sintering. It combines the hardness and wear resistance of a ceramic material, most commonly tungsten carbide (WC) with the toughness provided by a ductile binder phase, e.g. cobalt [16]. The microstructure of a metal cutting tool made from cemented tungsten carbide is shown in Fig. 6. It consists of an interconnected skeleton of WC grains (bright) and a cobalt-binder (dark), shown as pockets in-between the WC grains. Due to its anisotropic structure, WC crystals develop anisotropic shapes in form of flat triangular prisms with truncated edges [17]. The average carbide grain size of conventional cemented carbides used in metal cutting is in the range of 0.5 to 4 μm with around 5 to 20 vol.% binder phase [18]. Adjustment of the properties of cemented carbides can be done by changing the carbide grain size and binder content or by addition of other refractory carbides (e.g. TiC or TaC). In this way it is possible to attain the optimal combination of hardness, toughness and chemical stability required for the specific application [17].

Another way of optimizing the wear resistance and performance of cemented carbide cutting tools is the application of coatings by means of chemical or physical vapor deposition processes. Such tool coatings are usually up to a few micrometers thick and consist of ceramics e.g. oxides, nitrides, or carbides [18]. They can consist of a single layer or of a combination of multiple layers. An example of a coating can be seen in Fig. 6b.

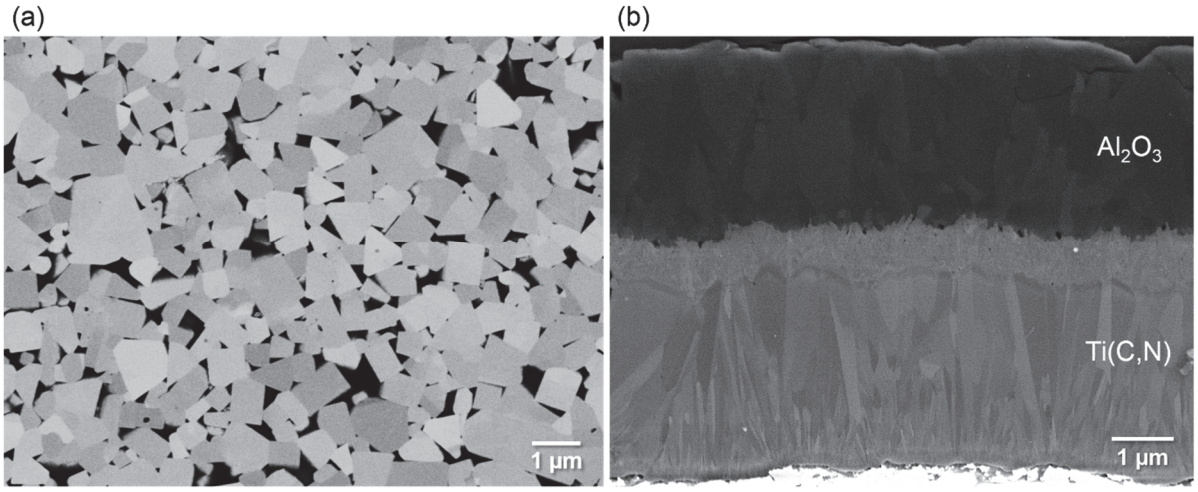

Fig. 6: Micrographs of the microstructures of (a) a cemented tungsten carbide cutting tool with its interconnected skeleton of WC grains and binder phase (black) and of (b) a ceramic coating deposited on a cemented carbide cutting tool.

3.2 Tool wear forms

The conditions in the cutting zone (see section 2.2) lead to severe tribological conditions at the interface between workpiece and tool. The tool is therefore inevitably subjected to wear which ultimately determines its service life. Ideally, when cutting a certain material, the tool material and cutting parameters are chosen so that the tool wear increases in a steady and controllable way.

The most common wear form in metal cutting is flank wear which develops on the major and minor cutting edge (see Fig. 7a). The major cutting edge is the part of the cutting tool where the chip is formed, whereas the minor cutting edge is at the nose of the tool where the surface of the machined part is produced. Progressing flank wear leads to a larger contact area between the tool and the newly generated workpiece surfaces which results in increased heat generation in the tertiary shearing zone. It furthermore affects the resultant force, mainly by increasing the feed and/or passive force [6]. The most common way to quantify flank wear is by measuring the width of flank wear (VB), which is measured on the major cutting edge, see Fig. 7a. The typical development of flank wear as a function of cutting time for two levels of cutting speed is illustrated in Fig. 8. Flank wear usually develops in three stages: it starts with an initial running-in phase (Stage I), is followed by a phase of steady wear (Stage II), and finally results in accelerated wear (Stage III) [19]. The rate of flank wear depends on different factors, including the cutting parameters (e.g. cutting speed, as illustrated in Fig. 8), the employed cutting insert, and the workpiece characteristics [19], with the latter one being the main focus of the present work.

Another wear form which can develop on the flank face of the cutting tool is notch wear. The example in Fig. 7a shows a notch at the depth of cut line on the major cutting edge.

Crater wear (see example in Fig. 7b) occurs on the rake face in the contact zone between chip and cutting tool. With its progression, the load bearing capability of the tool decreases and the cutting edge becomes more prone to sudden failure by plastic deformation or fracture [18].

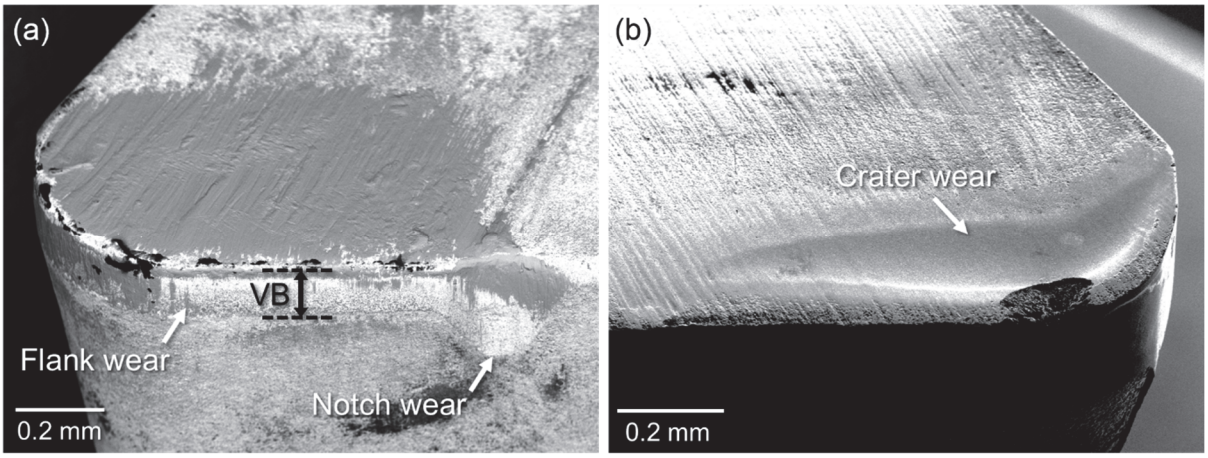

Fig. 7: SEM micrographs showing the major cutting edges of worn metal cutting tools exhibiting commonly observed wear forms: (a) Flank wear (width of flank wear land indicated by "VB") and notch wear; (b) crater wear on the rake face of the tool. The tool in (b) was etched to remove adhered workpiece material in order to make the crater visible.

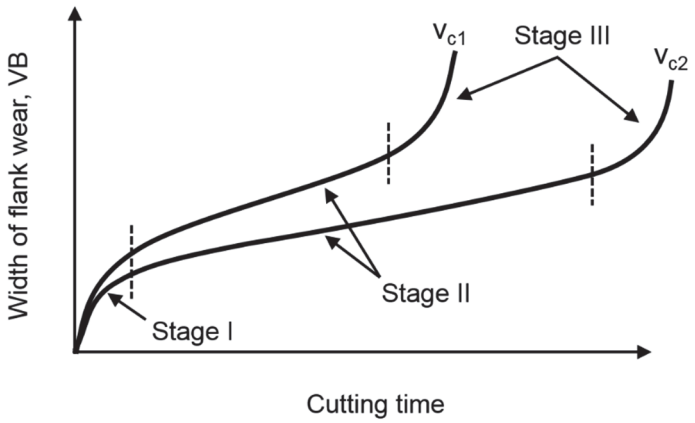

Fig. 8: Typical progression of flank wear plotted as a function of cutting time for two levels of cutting speed ($v_{c1}>v_{c2}$).

Flank, crater, and notch wear are gradually developing wear forms, whereas fracture or cutting edge depression by plastic deformation usually occur suddenly and can lead to total failure of the cutting tool. Examples of these two wear forms are shown in Fig. 9.

Plastic deformation of the cutting edge is caused by exceedingly high mechanical and thermal stresses acting on the tool [20], [21]. As illustrated in Fig. 9a, gross deformation can lead to a depression or displacement of the cutting edge towards the flank face [6]. These geometrical changes of the rake and flank angles can change the thermo-mechanical conditions at the tool surface [20] and by that lead to accelerated wear or sudden failure by fracture of the tool [22]. The micrograph in Fig. 9b shows a tool which has failed by fracture of the whole cutting edge.

In general, tool wear has a negative effect on machined surfaces by impairing the dimensional accuracy and surface integrity of the produced part. In order to meet the part requirements, it is therefore necessary to replace worn tools before a certain level of wear is reached [23]. In practice, a certain maximum width of flank wear land is often set as the criterion of maximum allowed tool wear [18].

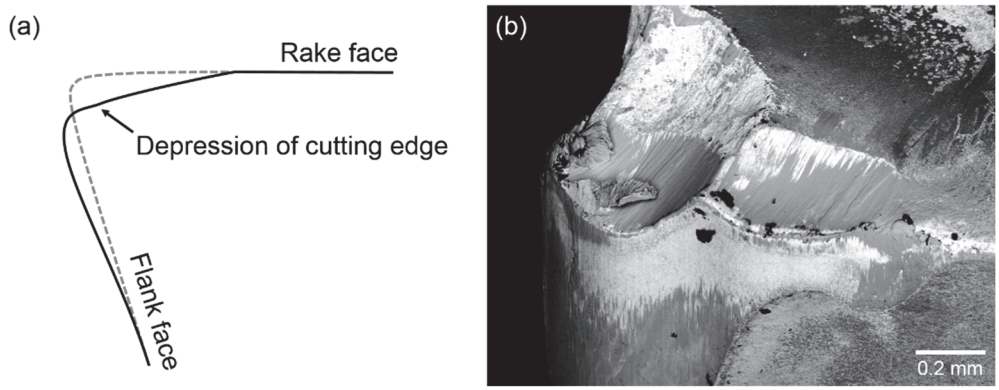

Fig. 9: Examples of (a) depression of the cutting edge by gross plastic deformation, and (b) a cutting tool which failed by fracture.

3.3 Tool wear mechanisms

The overall wear of cutting tools is generally considered to be due to several wear mechanisms being active at the same time, often with one dominating mechanism which controls the overall tool wear. The relative contribution of the individual mechanisms depend on e.g. the mechanical, thermal, and chemical properties of the tool and workpiece materials as well as the amount of generated heat and mechanical loads in the cutting zone [24].

This section is discussing the most common tool wear mechanisms in metal cutting. It is important to differentiate the term "wear mechanism" from "wear form" (described in section 3.2): Wear mechanisms are the underlying processes responsible for the tool wear forms, i.e. the loss of tool material and the change of cutting tool geometry. Schematics of some of the respective mechanisms are provided in Fig. 10 and more detailed descriptions follow below.

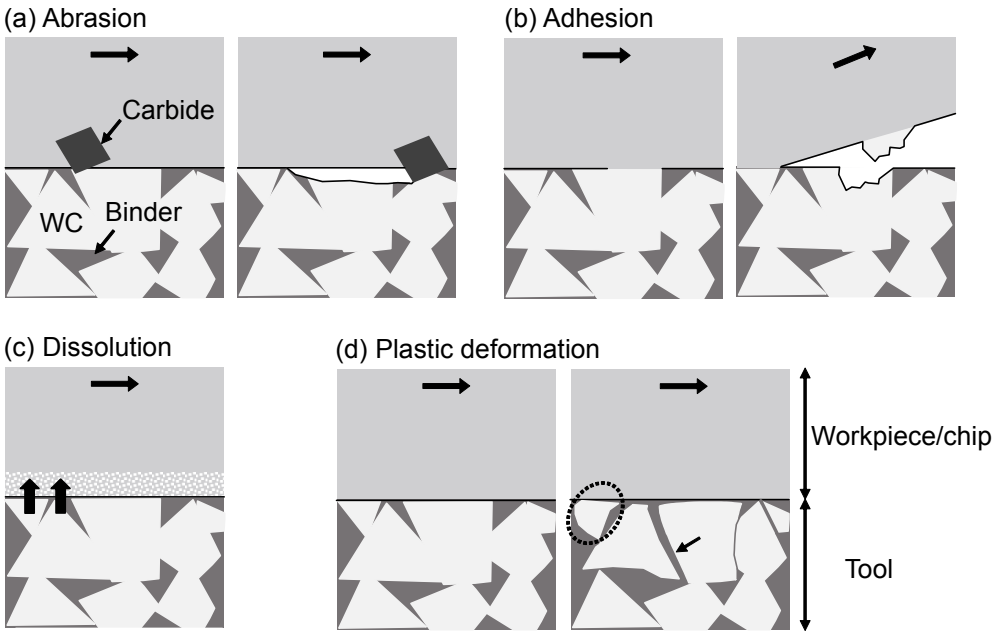

Fig. 10: Examples of different tool wear mechanisms at the interface between tool and workpiece/chip during metal cutting: (a) workpiece-carbide sliding against tool surface leading to removal of tool material; (b) localized adhesion between tool and workpiece followed by pull-out of tool material; (c) loss of tool material by chemical dissolution of its atoms into the workpiece/chip; (d) plastic deformation of WC grains (example encircled) and of the carbide network by WC grain boundary sliding (see arrow for example).

Abrasive tool wear

Wear by abrasion involves removal or displacement of material from a surface by hard particles or hard protuberances which are forced against the surface under simultaneous relative movement [25], [26]. The rate of abrasive wear increases with increasing hardness of the abrading particle relative to the abraded material. It has been shown that most severe abrasive wear takes place when the hardness ratio of abrading and abraded material is above 1.2 [25] or 1.25 [27], [28]. In addition to its hardness, the shape and size of abrading particles affect abrasive wear. Larger particles exert proportionally more wear than smaller particles. Similarly, rounded particles cause less abrasion than angular ones with pointy/sharp edges [25].

In metal cutting, abrasive wear of tool materials mainly occurs due to hard phases or particles present in the workpiece material being cut that slide along the tool surface on either the flank or as part of the chip on the rake face of the cutting tool [6]. Such hard particles can be carbides or

non-metallic inclusions such as oxides or nitrides which are commonly present in many alloys. During cutting, both the cutting tool material and the hard particles are subjected to thermal softening due to the high temperatures present in the shearing zones [21]. It is therefore the high temperature hardness of the material pair which determines whether the particle can abrade the tool material.

Since the unique tribological conditions encountered in metal cutting are hardly possible to mimic with tribometers such as pin-on-disc setups, several researchers have studied abrasive wear under metal cutting conditions, i.e. by conducting actual machining tests. For example, Ramalingam and Wright [29], Halila et al. [30], and Binder et al. [31] have conducted cutting tests on workpiece materials with varying fractions of hard particles. All these studies reported that the tool wear rate increased with the amount of hard particles in the workpiece which was explained by increasing abrasive wear.

Wear by dissolution

In the cutting zone, elevated temperatures and intimate contact between mating tool/workpiece surfaces can promote the thermally activated wear process of diffusion/dissolution [6]. Varying terminologies are used in literature (e.g. "diffusion" or "dissolution") for this mechanism [6].

Regardless of the used terminology, the general concept is based on transport of atoms across the interface between the tool and the workpiece/chip in the cutting zone. The transport of tool-atoms into the moving chip or workpiece on the rake and flank face of the tool, respectively, leads to loss of tool material [6], [23].

Several researchers argue that this mechanism is better described by the concept of dissolution rather than diffusion [21], [32], [33]. For example, Wong et al. [32] discuss that diffusion is a volumetric effect whereas dissolution is an interfacial mechanism occurring locally at the interface between tool and workpiece/chip. This is furthermore backed up by Kramer and Suh [33] who state that the tool wear rate is independent of the diffusion characteristics of the tool material in the workpiece material. The basic idea behind this argumentation is that the very short contact times encountered in the cutting zone during machining (< milliseconds) do not allow atoms of the tool to diffuse significant distances into the workpiece/chip. Instead, dissociation of tool material is followed by atomic dissolution into a very narrow region of the fast-moving chip/workpiece.

Based on this concept, some authors have used thermodynamic approaches to estimate the solubility of various tool and coating materials in different machined workpiece materials [21], [28], [32]–[34] which enabled them to predict tool wear and rank the resistance of various tool and coating materials against wear by dissolution. Accordingly, a tool material with low solubility in the workpiece indicates high resistance against dissolution wear and hence little contribution of this mechanism to tool wear. In contrast, wear by dissolution should play a more significant role when the respective solubility is comparably higher.

According to Kramer [34] and Olortegui-Yume and Kwon [35], the chemical solubility of a tool material depends on the compound's free energy of formation and the excess free energies of solution of the individual constituents in the respective machined workpiece and the interface temperature in the cutting zone [34]. It is therefore proposed that the relative importance of tool wear by dissolution for a certain pair of tool and workpiece material increases with increasing cutting speed, the main factor affecting the temperature in the cutting zone [23].

Additional to dissolution of tool material into the chip/workpiece material, machining of highly reactive materials like titanium alloys can lead to chemical reactions between titanium and the tool material. For example, when using cemented carbide cutting tools, formation of layers of TiC at the tool-workpiece interface have been reported together with carbon depletion of WC grains [36],

[37]. When present at the workpiece-tool interface during cutting, such reaction-layers can significantly affect the wear behavior of the tool by e.g. changing the dissolution process [21] or altering the mechanical properties of the tool locally [36].

Adhesive wear

Wear by adhesion is caused by localized bonding between contacting solid surfaces leading either to material transfer between the two surfaces or to loss from one of the surfaces [26].

During metal cutting operations, the workpiece/tool interface in the cutting zone is characterized by very high contact pressures (up to 2-3 GPa [14]). Consequently, the real area of contact constitutes a large portion of the apparent contact area between the tool and the workpiece [23]. This tight tool-workpiece contact in the cutting zone can promote the formation of micro-welds between the mating materials. During relative tangential movement between tool and workpiece, material-separation can occur in the tool rather than at the interface between tool and workpiece. In that case, part of the tool material is torn away and removed as fragments [6], [23].

Adhesion is also the underlying mechanism for built-up edge formation [6]. This phenomenon can generally be observed at relatively low cutting speeds. Transferred workpiece material accumulates on the tool rake face and can remain temporarily stable. This accumulation of material can take over the function of the cutting edge and will result in a change of the geometry of the cutting edge. Depending on the cutting conditions, the built-up layer gets periodically broken off and transferred to the machined workpiece surface or to the chip which can impair the surface finish [6].

Plastic deformation

Depending on the tool material and the thermal and mechanical loading, the macroscopic deformation of the cutting edge described in section 3.2 can take place by one or a combination of several deformation mechanisms on the microscopic level. In case of cemented tungsten carbides these mechanisms are plastic deformation of the binder phase, plastic deformation of WC grains, and plastic deformation of the WC network by grain boundary sliding [38], [39].

Oxidation

The high temperatures generated in metal cutting facilitate oxidation processes where the tool material and/or workpiece material locally react with the surrounding air [6]. The formed reaction products can either be removed by the moving chip/workpiece or stay attached to the tool surface as an transfer layer [6]. Such oxygen-rich transfer layers have shown to change the tool wear behavior both positively and negatively depending on the used tool and workpiece material [40], [41].

4 Workpiece properties and their influence on the cutting process

This chapter deals with workpiece material properties and their effect on the metal cutting process, mainly in terms of thermal and mechanical loads on the tools as well as tool wear.

Table 1 contains some thermal and mechanical properties of three workpiece materials, a low-alloy steel, a stainless steel, and a superalloy (in two different conditions). The table exemplifies how workpiece-properties can be used as an indicator for the general machining behavior when cutting different material types [18]. For a more comprehensive description of the material behavior and resulting tool loads, dynamic stress-strain data obtained at appropriate temperatures and strain-rates would be required together with temperature-dependent thermal properties [42].

According to Table 1, the workpiece-properties can vary significantly depending on the type of material (compare for example low-alloy steel with stainless steel) but also depending on the condition (compare Alloy 718 in solutionized and hardened condition). These macro-properties and their variation have significant influence on machining and can explain the necessity of employing different ranges of cutting data and tools when different types of materials are machined.

Thermal conductivity and specific heat capacity of the workpiece both affect the temperature in the cutting zone [18]. Machining a workpiece material with low thermal conductivity generally leads to high cutting temperatures because of limited heat-conduction via the workpiece. Similarly, low specific heat capacity of a workpiece material results in high thermal loads in the cutting zone. Exceedingly high temperatures in the cutting zone usually lead to accelerated wear and/or plastic deformation of the tool. Workpiece materials with such thermal characteristics (e.g. Alloy 718) therefore generally require use of comparably low cutting speeds or feed rates or optimization of cooling and lubrication in order to lower the heat generation in the cutting zone [18].

Tensile strength and yield strength of a workpiece describe the material's resistance against deformation and fracture [18]. These two properties can therefore give indications about the cutting resistance/specific energy (i.e. the mechanical work/energy per unit volume of material removal) and the mechanical loads acting on the tool during cutting. Furthermore, since the majority of mechanical work during cutting is converted into heat (see section 2.2), the cutting resistance also affects the cutting temperature. Cutting a workpiece material with high tensile and yield strength (e.g. hardened Alloy 718) therefore generally results in high thermal and mechanical loads on the cutting tools which again favors the use of low cutting speeds and/or feed rates in order to achieve reasonable tool life.

Other factors influencing a material's cutting behavior are strain-hardening and ductility (i.e. elongation to fracture). The latter one is related to the material's tendency to adhere to the tool surface [18].

All the above mentioned aspects are related to "macro-properties" of the workpiece material. Besides, the workpiece-microstructure can also have an influence on the cutting process, e.g. when machining workpieces with similar macro-properties but with varying microstructures. For example, increasing grain size has shown to significantly increase the tool notch wear and to influence chip formation in case of machining different types of metallic workpiece materials [43]–[46].

In another study, the effect of the amount of oxide particles added to a ferritic-pearlitic steel on the tool wear during turning was investigated [31]. Despite the steel's macro-hardness remaining nearly constant, a significant increase in flank wear was observed for increasing amounts of oxide particles added to the steel [31]. Additionally to carbides, different types of non-metallic inclusions (e.g. sulfides and oxides) can play a crucial role regarding tool wear when machining steels.

Depending on their composition and resulting properties, such inclusions have been reported to be both beneficial and detrimental for tool life [47]–[51].

Table 1: Comparison of mechanical and thermal properties of some alloys at room temperature [52].

Material type (alloy name, condition)	Thermal conductivity [W/(mK)]	Specific heat capacity [J/(kgK)]	Yield strength [MPa]	Tensile strength [MPa]	Elongation to fracture [%]
Low-alloy steel (AISI 4820, annealed)	35 - 50	460 - 500	410 - 515	610 - 750	18 - 27
Stainless steel (316L)	13 - 17	490 - 530	205 - 310	515 - 620	30 - 50
Superalloy (Alloy 718, solutionized)	11.6 - 12.6	440 - 458	724 - 800	827 - 914	35 - 50
Superalloy (Alloy 718, hardened)	11.6 - 12.6	440 - 458	1000 - 1110	1170 - 1320	10 - 15

5 Experimental details and analysis techniques

In this chapter, the investigated workpiece materials and the reported tool wear responses during machining are presented. Additionally, the used tools along with the setups of the machining tests are stated. Finally, the characterization techniques used to study the workpieces and the worn tools are explained.

5.1 Workpiece materials

Vanadis 10 tool steel

Tool steels are a group of highly-alloyed steels which exhibit high hardness and high resistance against abrasive wear under severe working conditions. This makes them suitable to be used for tooling in cold- and hot-forming applications [53].

Tool steels are alloyed with strong carbide-forming elements like Cr, Mo, V, or W. Controlled formation of high fractions of the desired carbides occurs during solidification of the alloy as well as during subsequent processing and heat treatments. In order to achieve the desired final properties, tool steels are usually heat treated by austenitizing, martensitic hardening and finally by tempering [53].

The Vanadis 10 steel used in this study was processed via the powder metallurgy route and had a composition of 2.99% C, 0.60% Si, 0.42% Mn, 8.05% Cr, 1.51% Mo, 9.99% V, 0.17% Ni, 0.018% S, 0.15% N (all in weight percent, wt%). The powder metallurgy process gives the material a very homogenous structure and a very low amount of non-metallic inclusions [54]. The workpiece was tested in soft, ferritic condition.

316L austenitic stainless steel

Stainless steels are a group of alloys which offer high resistance against corrosion which they owe to large amounts of Cr (>12 wt%) added as an alloying element. The enhanced corrosion-resistance stems from Cr being able to form a thin, stable and adherent oxide layer on stainless steel surfaces. This oxide layer effectively passivates the steel surface and thereby provides protection from corrosive species [53]. Austenitic stainless steels such as 316L are alloyed with sufficient amounts of Ni (usually > 8 wt%) which stabilizes and preserves austenite at room temperature.

In this study, two bars of 316L were investigated (Workpiece A and Workpiece B). Their compositions are given in Table 2. The two bars were obtained from different suppliers. Both bars were Ca-treated for enhanced machinability. Ca-treatments transform hard oxide inclusions in the steel (e.g. Al_2O_3) into softer, Ca-containing oxides [50].

Table 2: Composition (wt%) of the investigated 316L austenitic stainless steel bars.

Element	C	Si	Mn	P	S	Cr	Ni
Workpiece A	0.010	0.25	1.73	0.030	0.027	16.74	10.05
Workpiece B	0.021	0.57	1.47	0.030	0.025	16.91	10.07
Element	Mo	N	Ca	O	Ti	Al	Mg
Workpiece A	2.02	0.047	0.015	0.0203	<0.001	0.008	<0.001
Workpiece B	2.14	0.057	0.015	0.0125	0.009	0.007	<0.001

20MnCrS5 case-hardening steel

This type of steel is applied in components which require high hardness and wear-resistance at the surface while having high toughness in the core. Such steels usually have a base-carbon content of around 0.2 wt% [53]. Surface-hardening is done by e.g. carburizing which increases the carbon content locally and hence enhances the surface-hardenability of the steel part [53]. Typical components made from case-hardening steels are gears, spindles, or camshafts.

The machined bar of 20MnCrS5 was not surface-hardened, i.e. it was machined in soft, ferritic-pearlitic condition [55]. Its composition was 0.205% C, 0.19% Si, 1.32% Mn, 0.018% P, 0.032% S, 1.31% Cr, 0.08% Mo, 0.15% Ni, 0.18% Cu, 0.025% Al, 0.015% Co, 0.011% N (all in weight percent, wt%) [55], [56].

Alloy 718 and Waspaloy

These alloys are part of the material class called superalloys. Due to their excellent combination of high-temperature strength, toughness, and high resistance against corrosion and oxidation, superalloys are used in turbomachinery components operating at elevated temperatures. Most notably, superalloys are a key factor of modern aircraft engines where they typically constitute around 40-50% of the total engine's weight [57]. Due to its use in safety-critical components, superalloys have to meet stringent material and machining-induced surface integrity requirements.

Due to its relatively large iron content, Alloy 718 is often classified as a nickel-iron based superalloy [58]. The alloy can be precipitation-hardened by use of appropriate ageing heat treatments. In hardened conditions, its microstructure contains intermetallic compounds, primarily gamma double prime (γ"), as well as lower fractions of delta phase (δ), and gamma prime (γ'). Furthermore, different carbides, like MC-type primary carbides are commonly present in the microstructure of Alloy 718 [58].

Waspaloy on the other hand is alloyed with comparably lower amounts of iron and is therefore a nickel-base superalloy. Its intermetallic strengthening phase is γ' and it additionally contains different carbides (e.g. MC, $M_{23}C_6$) [58].

The two workpieces in this study were age-hardened prior to the machining tests and their compositions are summarized in Table 3.

Table 3: Composition of investigated superalloy workpieces in wt% with nickel as balance.

	Cr	Co	Fe	C	Mo	Al	Ti	Nb	B	Mn	Si
Alloy 718	18.4	0.3	17.5	0.04	3.0	0.6	0.9	5.5	0.001	0.09	0.05
Waspaloy	19.4	13.2	1.2	0.03	4.1	1.3	3.1	-	0.005	0.03	0.05

5.2 Cutting tools

In this work, the substrates of all cutting inserts consisted of cemented tungsten carbide. The majority of the tests was conducted using the tools in uncoated condition. Two different substrate-grades were used. The choice of uncoated inserts was made since the characterization of wear and adhered layers on coated tool surfaces would add complications to the correct assessment of the wear topography and composition of adhered layers (e.g. thin oxygen-rich adhesion layers on top of an alumina coating).

Complementary tests using coated tools were done for some cutting conditions in case of turning the tool steel and the austenitic stainless steel and are presented in Paper I. The specifications of the used tools are summarized in Table 4.

Table 4: Some specifications of the employed cutting tools.

ISO code	**TCMW 16 T3 04**	**TPUN 16 03 04**
Substrate grade	Cemented carbide, 10% Co-binder	Cemented carbide, 6% Co-binder
Coating	Uncoated	Uncoated/coated*
Insert shape	Triangular	Triangular
Nose radius	0.4 mm	0.4 mm
Chip breaker geometry	None	None
Whiper geometry	None	None

*CVD-coated with TiCN-Al_2O_3, results presented in Paper I

5.3 Turning tests

The machining tests presented in this thesis were performed using an EMCO Emcoturn 365 CNC turning machine. In case of the superalloy workpieces, face turning test were carried out while longitudinal turning tests were done for the steel workpieces. The aim of the turning tests was to monitor and compare the steady-state flank wear when machining the different workpieces. Since the machined material types exhibit different mechanical and thermal properties, carefully selected and varied ranges of cutting data were employed for the respective tests. A summary of the used cutting data is presented in Table 5.

The turning experiments were done in predefined, controlled intervals. Between every interval, the machine was stopped and the flank tool wear was measured by using a stereo optical microscope (Zeiss Discovery V20). Since this is the most commonly observed wear form in metal cutting and as it was present for all types of workpiece materials in the present study, focus was placed on the maximum width of flank wear land (VB). An arrangement of stereo optical micrographs which exemplifies the increase of tool flank wear with machining time is shown in Fig. 11.

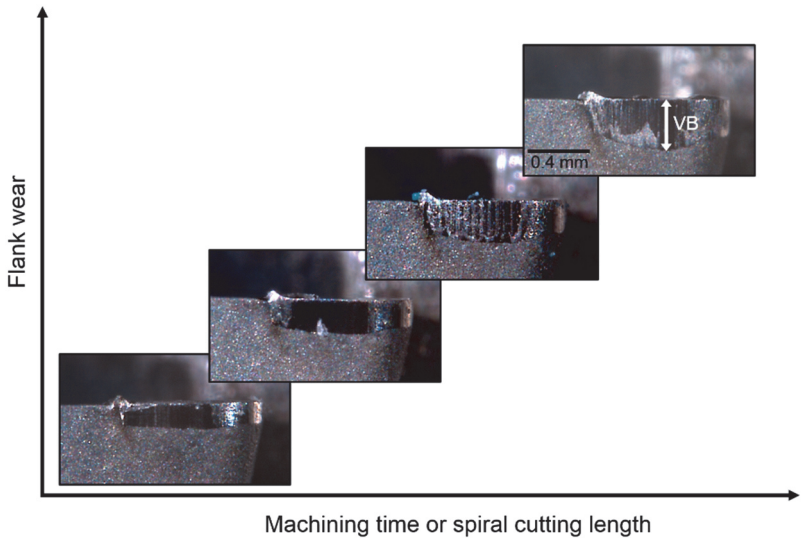

Fig. 11: Arrangement of stereo-optical micrographs of the major cutting edge of an uncoated cutting insert exemplifying the progression of flank wear (VB) with increasing machining time. The micrographs were obtained when machining Vanadis 10 tool steel with 80 m/min cutting speed, 0.05 mm/rev feed rate, and 1 mm depth of cut.

Additionally to the tool wear, cutting forces were measured using a piezoelectric three component dynamometer (Kistler 9275A). In that way, the three force components were recorded and the respective average main cutting force (F_c), average feed force (F_f), and average passive force (F_p) was determined for each machining interval.

Table 5: Summary of the turning tests on the different workpiece materials. The main process parameters are cutting speed (v_c), feed rate (f), and depth of cut (a_p). The cutting angles are a result of the used tool holders.

	Vanadis 10	**316L**	**Alloy 718**	**Waspaloy**	**20MnCrS5**
v_c [m/min]	40, 80	120, 160	30, 45	45	120, 240
f [mm/rev]	0.05	0.08	0.05, 0.075, 0.1	0.05, 0.1	0.075
a_p [mm]	1	1	1	1	1
Tool	TPUN160304	TPUN160304	TCMW16T304	TCMW16T304	TCMW16T304
Rake angle [°]	5	5	0	0	0
Clearance angle [°]	6	6	7	7	7
Entering angle [°]	91	91	91	91	91
Nose radius [mm]	0.4	0.4	0.4	0.4	0.4
Coolant	Emulsion (6%)	Emulsion (6%)	Emulsion (6%)	Emulsion (6%)	Dry

5.4 Diffusion couple tests

To investigate whether there are differences in wear by diffusion/dissolution during cutting Alloy 718 and Waspaloy, static diffusion couple tests on both alloys and the cemented carbide tool material were conducted. For these tests, the same tool grade was used as in the corresponding machining tests on the superalloys. Even though the static contact condition between workpiece and tool is significantly different from the dynamic case during machining, diffusion couple tests can provide a qualitative comparison of this wear mechanism when machining the two superalloys.

Polished surfaces of samples of the superalloys and the cemented carbide material were brought in contact (about 24.5 MPa contact pressure) while being placed inside a furnace held at the respective test-temperature. During the tests, flowing nitrogen was used to prevent oxidation of the samples. A summary of the test conditions can be seen in Table 6. After the tests, the diffusion couples were cross-sectioned and metallographic specimens were prepared by use of conventional grinding and polishing. The specimens were examined at the superalloy/tool interface using scanning electron microscopy and Auger-electron spectroscopy.

Table 6: Overview of test conditions during static diffusion couple tests on the superalloys.

Workpiece/tool material	Temperature [°C]	Time [min]	Contact pressure [MPa]
Alloy 718/WC-Co	800, 1000	90	~24.5
Waspaloy/WC-Co	800, 1000	90	~24.5

5.5 Microstructure and wear characterization

5.5.1 Scanning electron microscopy and associated techniques

A major part of the presented work was dedicated to characterization of the studied workpiece materials and worn tools using scanning electron microscopy (SEM). In SEM, a finely focused electron beam is scanned across the specimen surface in a scan raster [59]. The incident electrons interact with the atoms of the specimen leading to the formation of different types of signals which can be detected and used for imaging and analysis.

- Secondary electrons (SE) are used for imaging the specimen's topography. SEs are outer shell electrons which are ejected from atoms of the specimen due to inelastic scattering of primary beam electrons. SEs have low kinetic energy (< 50 eV), therefore only the SEs from comparably shallow depths beneath the surface are able to escape the specimen [59].
- Backscattered electrons (BSE) are electrons of the primary electron beam which have been scattered elastically. As they do not lose much energy, they can escape from deeper within the specimen. Furthermore, the yield of BSEs is dependent on the atomic number of the elements in the probed specimen with heavy elements having higher yield than light elements. It is therefore possible to obtain chemical contrast with help of BSEs (heavy elements appear bright and light elements dark) [59].

The obtainable spatial resolution of the SEM is dependent on the spot size of the focused electron beam as well as the size of the interaction volume. The interaction volume in turn is a function of the energy of the primary electron beam, the atomic number of the imaged material, and the tilt-angle of the specimen surface relative to the primary electron beam. For example, lower energy of the incident electrons, higher atomic number of the imaged material yield in a smaller interaction volume. Similarly, the interaction volume becomes smaller and asymmetric for increasing tilt of a specimen surface relative to the primary electron beam [59].

In this study, a FEI/Philipps XL-30 and a LEO Gemini SEM, both equipped with detectors for SE and BSE imaging were used. For the high-resolution imaging of worn tool surfaces and thin adhered layers, acceleration voltages between 1 to 5 kV were preferably used in order to limit the interaction volume and to decrease the sampling depth of the electron beam. In some cases, the used acceleration voltages were altered systematically (up to 20 kV), either to get an impression of the thickness of adhered layers, or to study the tool material underneath. In addition to imaging, energy-dispersive X-ray spectroscopy (EDS) and the electron backscatter diffraction (EBSD) technique were applied to get chemical and crystallographic information of the investigated specimens, respectively.

Energy-dispersive X-ray spectroscopy

Energy-dispersive X-ray spectroscopy (EDS) utilizes element-characteristic X-rays which are emitted upon interaction of the electron microscope's primary electron beam with the atoms of the probed specimen. Characteristic X-rays are generated when incident electrons are scattered inelastically and leave the atoms ionized through emission of inner shell electrons [59]. Such inner vacant electron sites can subsequently be filled by outer shell electrons and the atoms return to ground state. In this way, excess energy is released by X-ray photons. The energy of the emitted X-rays is defined by the energy difference between the electron shells involved in the process. The energy of emitted X-ray photons is therefore characteristic for the electronic structure of the element. By detection and measurement of energies of emitted X-rays, it is therefore possible to obtain qualitative and quantitative chemical information of the specimen [59].

Electron backscatter diffraction

The electron backscatter diffraction (EBSD) technique makes use of diffraction patterns generated when the focused electron beam interacts with a crystalline specimen. The specimen surface to be examined requires to be tilted toward the detector by approximately 70° relative to the horizontal. The diffracted electrons form flat cones of intensity (two parallel cones per atomic plane) above the tilted specimen [59]. These pairs of cones generate diffraction patterns when intercepting the phosphorous screen of the EBSD detector. A camera is used to acquire the diffraction patterns (also called Kikuchi pattern, see example in Fig. 12b). Such diffraction patterns consist of pairs of parallel Kikuchi lines. Their size and arrangement contain crystallographic information of the probed material. For example, pairs of Kikuchi lines (bands) represent planes in the crystal structure and places where bands intersect correspond to zone axes/crystallographic directions [60]. An automated computer system is used to detect the Kikuchi bands and their intersections in order to extract the crystallographic information. EBSD analysis can be done at specific locations (spots) or by scanning a predefined surface area of the specimen with a chosen step size to obtain orientation maps [59].

In the present work, EBSD was used for two purposes, namely phase discrimination and assessment of plastic strain. The latter was done using the local misorientation approach [61]. During plastic deformation of crystalline materials, dislocations form and lead to changes in the lattice orientation [62]. Local orientation differences can therefore give indications of the strain present in the material [61].

In this work, local orientation changes due to deformation were mainly presented by use of local misorientation maps created using the HKL Channel 5 software (Oxford Instruments). An example of a local misorientation map is shown in Fig. 12c. The color of each pixel represents the average orientation difference between this pixel and a set of pixels surrounding it [60]. The set of pixels surrounding the pixel of interest (see example in Fig. 12d) is also referred to as a kernel [61]. Orientation differences due to grain boundaries can be excluded and regions of higher local misorientation (i.e. strain) are highlighted. The local misorientation map in Fig. 12c was generated using a pixel filter size (kernel) of 3x3 and a subgrain exclusion angle of 5°, grain boundaries (>10°) are shown in white.

The crystallographic orientation of worn WC grain surfaces was examined in top-view after removal of adhered workpiece material by etching. The data was obtained with a HKL Nordlys EBSD detector (Oxford Instruments) using a step-size of 50 to 75 nm and an acceleration voltage of 20 to 25 kV for the primary electron beam. Post processing of the acquired EBSD data was done with the HKL Channel 5 software (Oxford Instruments). Additionally to the examination in top view, some tools were cross sectioned and analyzed after conventional metallographic sample preparation methods (grinding and mechanical polishing).

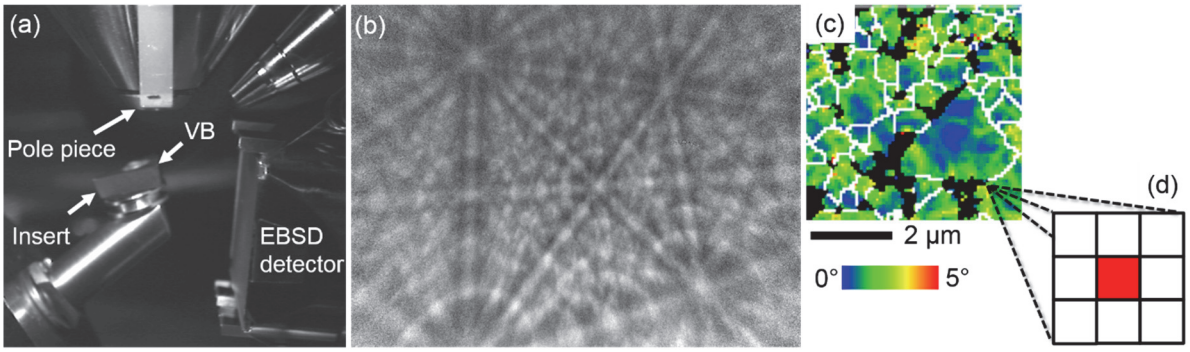

Fig. 12: Electron backscatter diffraction analysis of worn tool surfaces: (a) Setup in SEM with surface of flank wear land (VB) tilted 70° relative to the horizontal; (b) individual diffraction pattern obtained on deformed surface of a WC grain; (c) local misorientation map obtained on worn WC grains on a tool's flank wear land; (d) schematic of a 3x3 kernel used to determine the center pixel's average misorientation value.

5.5.2 Metallographic examination of workpieces

The machined workpieces were investigated for their microstructure and hardness. A schematic of the different aspects that were studied is provided in Fig. 13. Metallographic samples were taken from different positions in the workpieces and prepared using conventional grinding, polishing, and etching techniques. The investigations were focused on samples corresponding to longitudinal sections of the workpiece-bars.

Optical microscopy (Leitz DMRX) in combination with SEM/EDS/EBSD (see subsection 5.5.1 for details) were used to examine the samples. Depending on the studied microstructural aspect, samples were investigated either directly after polishing ("as-polished") or after etching using appropriate etchants (see Fig. 13). A modified Kallings Number 2 solution (1g $CuCl_2$ in 50 ml methanol, 25 ml water, and 25 ml hydrochloric acid) was used to reveal the microstructure of the superalloys. The tool and case-hardening steel were etched employing Nital (2-3% nitric acid in ethanol) and a solution of oxalic acid (10 g oxalic acid in 100 ml water) was used for the stainless steel bars.

Estimation of average grain size was done by use of the mean lineal intercept method [63]. Straight lines of known length were drawn on micrographs of the respective material and the number of grains intercepted by these lines were counted. The mean intercept length was obtained by dividing the test-line lengths by the number of intercepted grains. The length of the test lines and the magnification of the micrographs were chosen to yield a minimum of 50 intercepts per micrograph. Several micrographs were analyzed for each sample. In order to obtain accurate results, metallographic samples were examined after the grain structure was clearly visible. In case of the investigated superalloy samples, this was the case after etching. The 316L workpiece samples on the other hand were imaged in as-polished condition employing the BSE detector in the SEM.

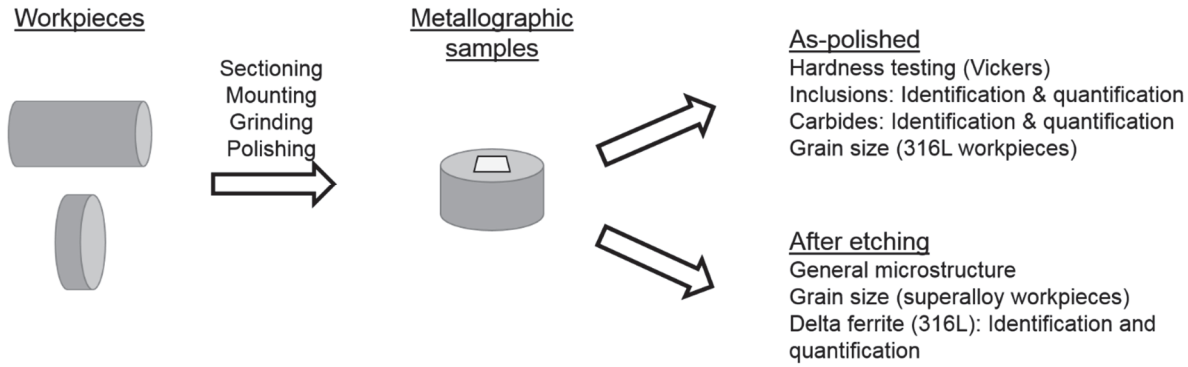

Fig. 13: Overview of metallographic examinations conducted on the machined workpieces.

As-polished samples were also examined with respect to their carbides and non-metallic inclusions. The different types of these phases were first determined using EDS point analysis. Quantification of their amounts was done on SEM images acquired using BSE. Contrast emerging from the different average atomic numbers of the different types of inclusions and the material matrices enabled to distinguish most types of carbides and non-metallic inclusions present in the different workpiece materials. The obtained micrographs were converted to binary images and the fractions of the respective phases were quantified using the image processing software ImageJ [64]. Fig. 14 contains a BSE image of a 316L specimen together with the respective binary images used for image analysis in order to determine the fraction of sulfide and oxide inclusions, respectively. The higher magnified inserts clearly show the possibility of distinguishing sulfide and oxide inclusions. Note that for illustration purposes, Fig. 14 shows only one quarter of one original high-resolution micrograph used for the quantification procedure in case of the 316L workpieces. The original micrographs display an area of 569 x 427 μm^2 at a resolution of 3072 x 2304 pixels.

The hardness of all investigated workpieces was determined on as-polished samples. A Wolpert Dia Testor 2 Rc hardness tester was used with 10 kgf test force and a Vickers indenter tip and the average of several indents was obtained for each sample.

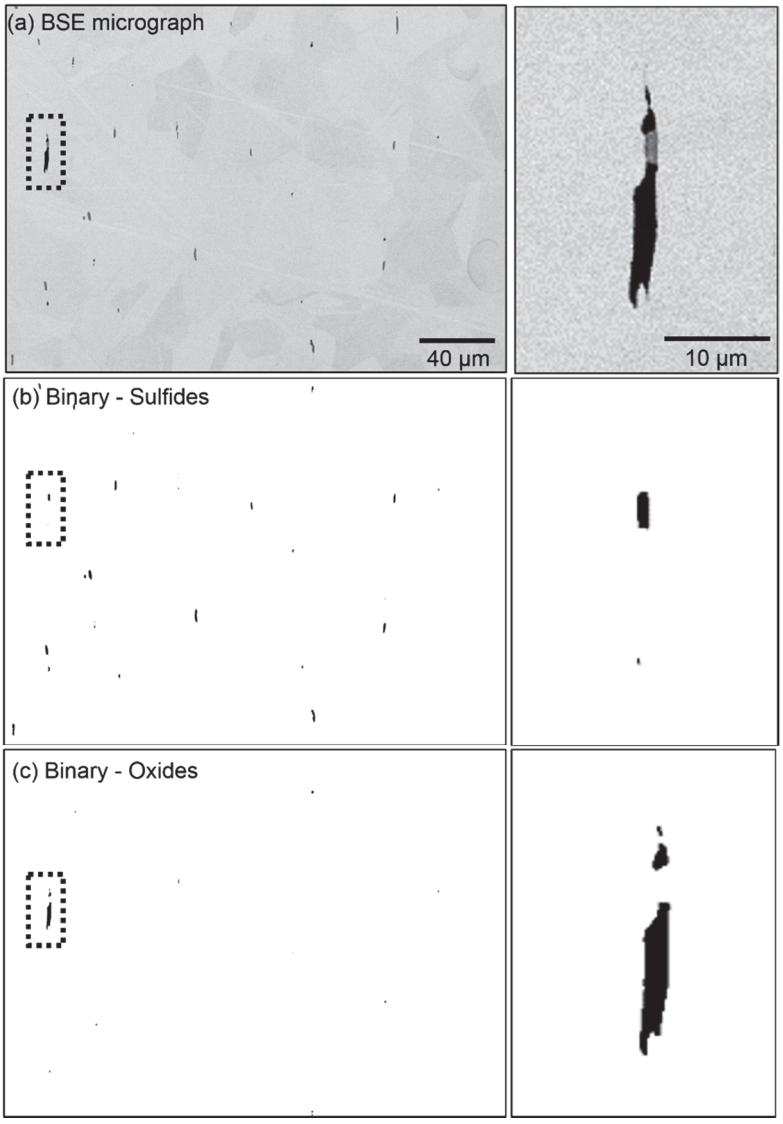

Fig. 14: Micrograph with corresponding binary images used to quantify the amount of non-metallic inclusions present in the 316L workpieces: (a) BSE micrograph with inclusions shown as darker patches; (b), (c) associated binary images with areas corresponding to sulfide and oxide inclusions displayed as black pixels. The inserts on the right display a zoomed-in view of a mixed inclusion containing both sulfide and oxide parts.

5.5.3 Preparation of worn tools

After the conducted machining tests, selected worn cutting inserts were characterized in two steps (see Fig. 15). In the first step, the tools were examined directly after the tests without further preparation, i.e. with adhered layers of workpiece material still present on the worn tool surfaces. At this stage the focus was put on the overall appearance of the cutting edge, the present wear forms (e.g. flank wear, notch wear) and the characteristics of adhered layers. To prepare the inserts for a more detailed examination, they were submerged in a solution of diluted hydrochloric acid (1 part concentrated hydrochloric acid and 1 part water) while the solution was kept at about 75 °C until the majority of the adhered workpiece material was etched away. In the subsequent, second characterization-step, the examination was focused on the microscopic wear features, i.e. topography and surface deformation of WC grains.

Some inserts were additionally investigated in cross-section. Cross-sections were prepared by use of conventional metallographic methods (mechanical sectioning with low-speed saw, grinding and polishing).

Additionally to the mainly SEM-based examination, the surfaces of selected inserts were investigated by use of white-light interferometry (Sensofar S Neox).

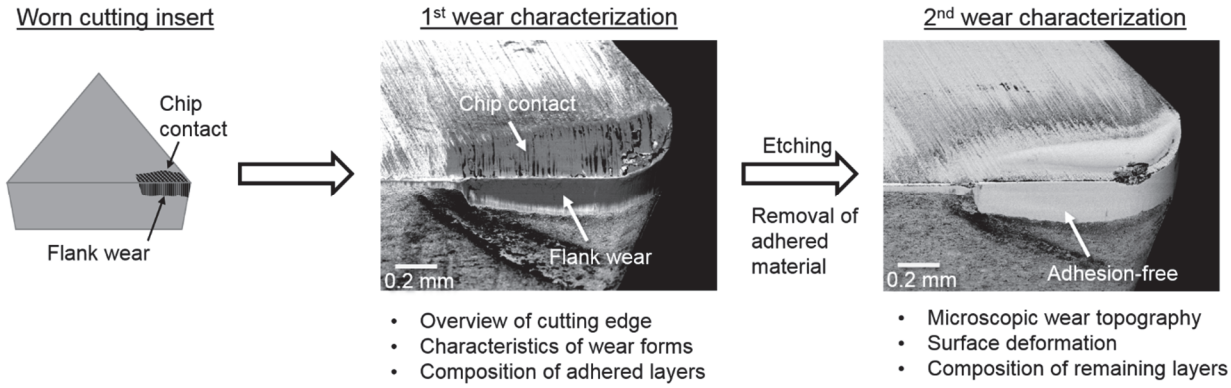

Fig. 15: Steps of SEM-based tool wear investigation conducted in this work. The micrographs show an uncoated insert after machining 316L austenitic stainless steel before and after etching in diluted hydrochloric acid.

6 Summary of experimental results and discussion

This chapter first gives a summary of the microstructures and characteristic constituents of the different workpiece materials tested within this work. Then, the results of the machining tests are presented in terms of the measured flank wear developments and cutting forces. Finally, the SEM-based characterization of worn cutting tools is summarized and discussed with respect to the workpiece microstructures. It should be noted that the following summary focusses on the results of uncoated tools.

6.1 Metallographic examination of machined workpieces

All machined workpieces were subjected to metallographic investigations with the main purpose to determine the respective microstructural characteristics (e.g. grain size, strengthening phases, type and amount of carbides and non-metallic inclusions) as well as the macro-hardnesses. Table 7 provides an overview of the main outcomes of the metallographic investigations carried out in this work.

Table 7: Main characteristics of investigated workpieces.

Material type	Machined alloy	Av. hardness [HV]	Av. hardness [GPa]	Particles present in microstructure
Tool steel	Vanadis 10	272	2.67	Carbides (MC, M_7C_3)
Superalloy	Alloy 718	430	4.22	Intermetallics (γ" precipitates, δ-phase, γ' precipitates), primary carbides (NbC), non-metallic inclusions (TiN)
Superalloy	Waspaloy	382	3.75	Intermetallics (γ' precipitates), primary carbides (TiC), non-metallic inclusions (TiN), $M_{23}C_6$ carbides
Case-hardening steel	20MnCrS5	164	1.61	Carbides (cementite), non-metallic inclusions (MnS, Al-rich oxides)
Stainless steel	316L (Supplier A)	154	1.51	Non-metallic inclusions (MnS and oxides)
Stainless steel	316L (Supplier B)	180	1.77	Non-metallic inclusions (MnS and oxides)

The characteristic microstructures of most of the investigated workpieces can be seen in Fig. 16. The tool steel contained high fractions of hard and abrasive carbides (about 16.2 vol% MC carbides and about 7.4 vol% M_7C_3 carbides with average diameters of 1-3 μm) in a ferritic matrix (see Fig. 16a and b).

The case-hardening steel which was machined in soft condition is shown in Fig. 16c and d. The ferritic-pearlitic microstructure of the same workpiece has previously been investigated and its amount of pearlite was quantified as 50.2 vol% [55]. As evident in the higher magnified micrograph, the pearlite consists of alternating lamellae of cementite (Fe_3C and ferrite. The overall cementite-content is estimated to be around 5.6 vol% in the present workpiece. Furthermore, this workpiece contained non-metallic inclusions in form of sulfides (MnS, around 0.15%), Al-rich oxides, and occasionally B-rich nitrides (together around 0.011%), see Fig. 16d.

The investigated superalloys contained intermetallic phases, carbides and non-metallic inclusions (see Table 7). Micrographs of one of the investigated alloys (Alloy 718) are shown in Fig. 16e and f.

In contrast to the case-hardening steel, the investigated Ca-treated austenitic stainless steel with its very low carbon content (less than 0.03 wt%) does not contain any pearlite. Furthermore, no Cr-rich carbides which can precipitate in the investigated alloy 316L [65] were found at the grain boundaries of the two workpieces. Instead the workpieces' microstructures consisted of an austenitic matrix with occasional presence of non-metallic inclusions (see Fig. 16g and h).

Evidently, the different material types (e.g. tool steel and superalloys) are characterized by different microstructural constituents. The variety of different microstructures and thermo-mechanical workpiece-properties should trigger different mechanisms at the tool/workpiece interface in the cutting zone and hence lead to different tool wear responses during machining of the different material types. The following subsections are focused on the study of the resulting flank wear response and the underlying wear mechanisms and their dependence on the type of machined workpiece and its microstructure.

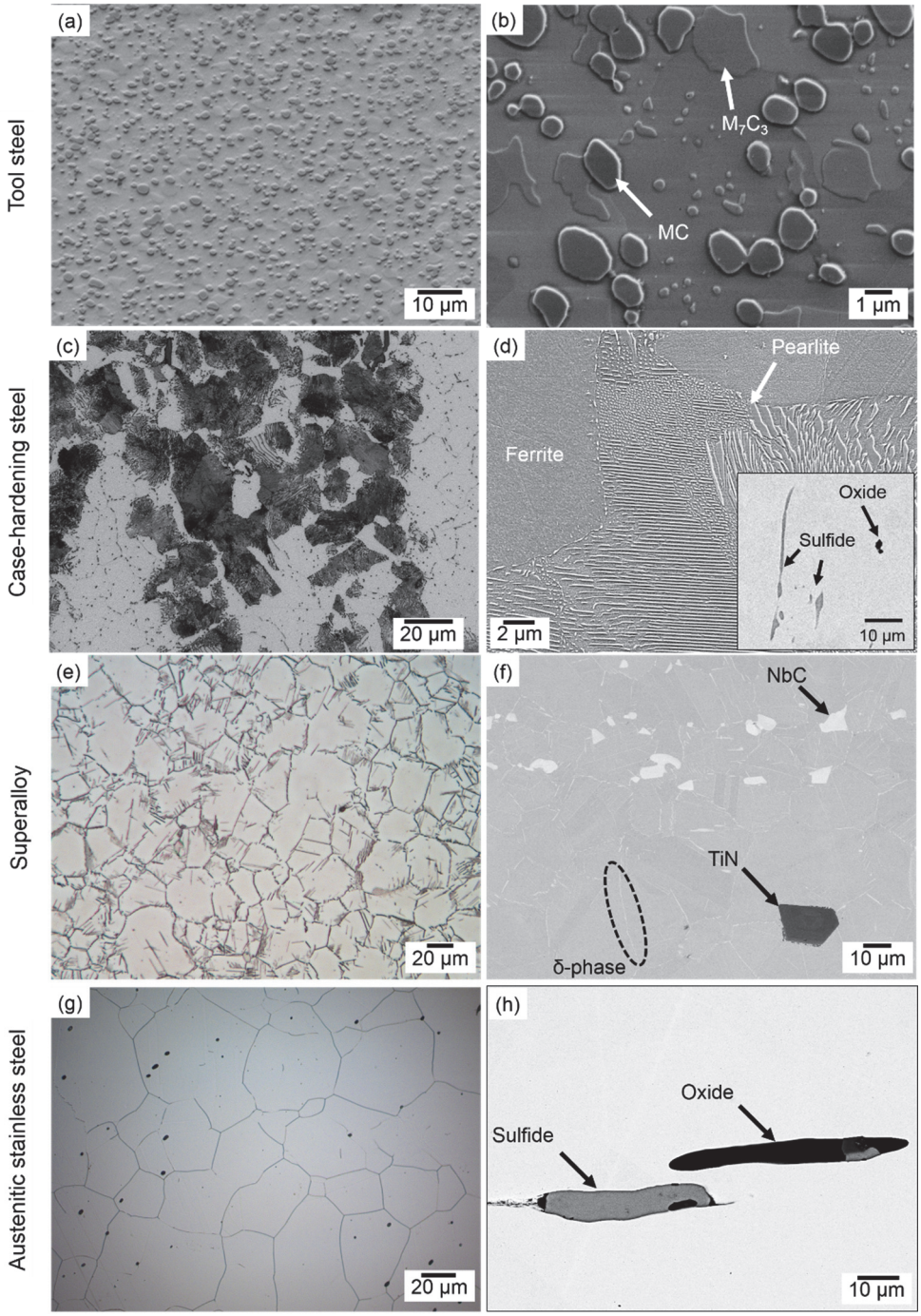

Fig. 16: Summary of representative micrographs showing the microstructures of some workpieces which were machined in this study: (a), (b) Vanadis 10 workpiece with hard, abrasive carbides in ferritic matrix; (c), (d) 20MnCrS5 with ferritic-pearlitic microstructure; (e), (f) wrought Alloy 718 with δ-phase, primary carbides, and TiN-inclusion; (g) 316L (Supplier A) with austenitic matrix and occasional presence of sulfide and oxide inclusions; (h) comparably large sulfide and oxide inclusions imaged at higher magnification.

6.2 Tool wear and cutting forces

This section summarizes the conducted turning tests on the various workpieces both in terms of flank wear development and cutting forces. The results of the tool wear tests are shown in Fig. 17 where the flank wear development as a function of spiral cutting length (SCL) is depicted. The results are grouped according to the type of machined workpiece material. Presenting the results as a function of SCL rather than cutting time enables for clearer comparison of tool wear results obtained when using significantly different cutting parameters which were applied for the different workpiece materials. The SCL essentially describes the distance the cutting tool travels relative to the workpiece surface during turning. As a complement, the corresponding total machining times are displayed next to the respective flank wear plots.

For the majority of the shown tests, fairly stable, gradual steady-state flank wear development can be observed. Machining one of the 316L workpieces was an exception where almost no increase in flank wear was seen throughout the entire test (see Workpiece B in Fig. 17c). Furthermore, machining of Alloy 718 using the higher feed rate resulted in accelerated, non-linear flank wear after about 110 m SCL (see Fig. 17d). As expected, when machining all alloys, increasing cutting speed (Fig. 17a-c) and increasing feed rate (Fig. 17d) generally led to a steeper increase in flank wear.

A significant difference in flank wear development can be seen when comparing the results of the two superalloys which were machined using two sets of identical cutting parameters (see Fig. 17d). In both cases, machining of Alloy 718 resulted in faster flank wear development as compared with Waspaloy. The same trend has previously been shown by Olovsjö and Nyborg [66] and Polvorosa et al. [67].

Surprisingly, despite the use of identical cutting parameters, a very significant variation of flank wear can also be observed when machining the same alloy (316L) from two suppliers (compare Workpiece A with Workpiece B in Fig. 17c). Machining of Workpiece A led to 0.3 mm flank wear width after about 1800 and 800 m SCL (or 15 and 5 min machining time) for the lower and higher cutting speed, respectively. During the same machining time, the flank wear width remained below 0.075 mm in case of both cutting speeds for Workpiece B.

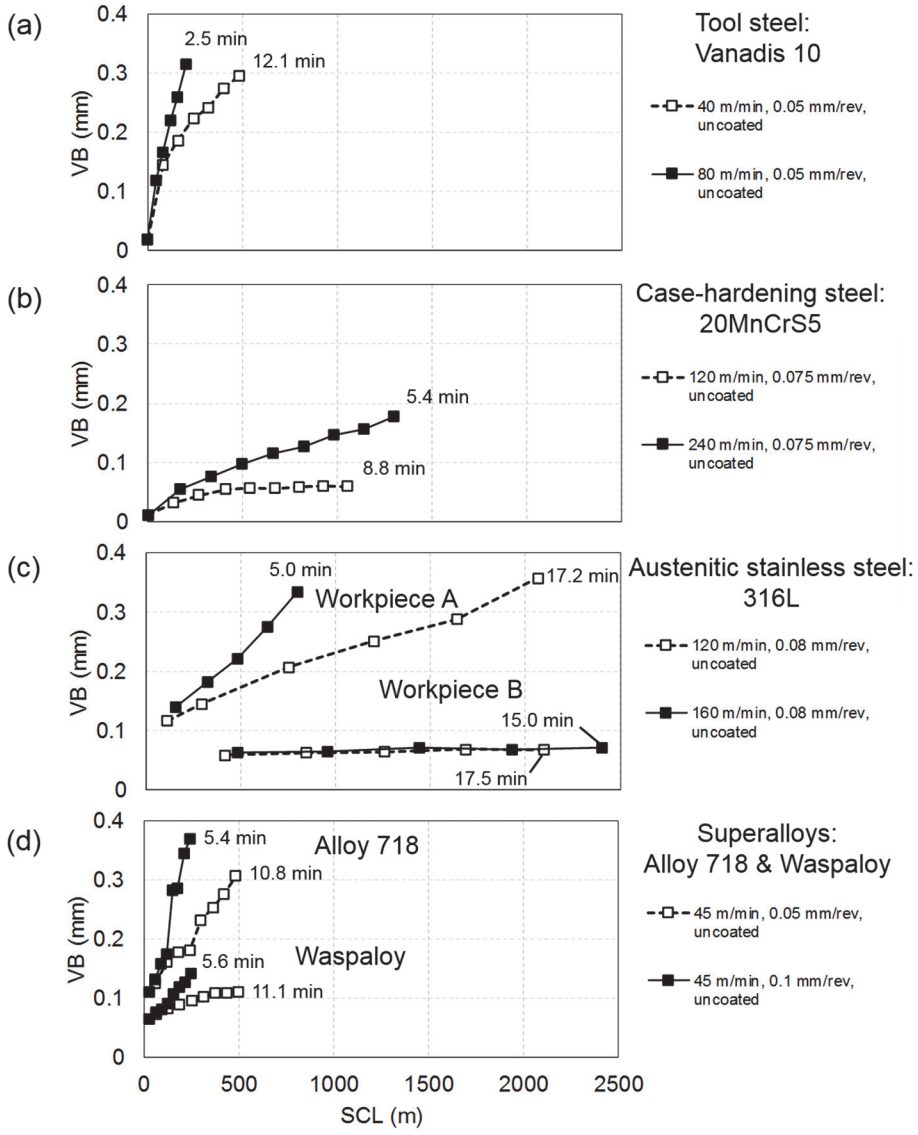

Fig. 17: Development of flank wear land width (VB) with increasing spiral cutting length (SCL) during tests when machining the investigated workpieces. Two workpieces of the same austenitic stainless steel ("Workpiece A" and "Workpiece B") were machined in (c). The used cutting speeds (in m/min) and feed rates (in mm/rev) are indicated together with the total machining time (in min) for the respective test. The depth of cut was constant (1 mm) for all tests. The data in (b) was adopted from [55].

Comparison of forces during cutting can give hints on the mechanical stresses acting on the tool surfaces. A summary of the cutting forces associated with turning the investigated materials can be seen in Fig. 18. All presented average forces were measured at the beginning of the first machining interval of the respective tests. The shown forces therefore represent the forces for unworn tools which enables to compare the forces without the influence of varying wear rates during cutting the different workpieces. Machining of all the steel workpieces resulted in main cutting forces in the range of 200 to 250 N under the investigated cutting parameters. Feed forces were in the range of about 100 to 150 N for all steels except for the case hardening steel 20MnCrS5 for which higher feed forces of about 175 N were recorded.

As compared to the steel workpieces, machining of the two superalloys generally resulted in higher cutting forces. The difference was less significant for the lower feed rate of 0.05 mm/rev (e.g. similar F_C as 316L machined with 120 m/min). For the higher feed rate of 0.1 mm/rev, however,

the difference between the superalloys and steels was more pronounced and all three force components were measured to be significantly higher than for cutting of all investigated steels.

The presented results of the flank wear development and the associated cutting forces emphasize the influence of the material characteristics of the workpieces on the cutting process. For example, despite significantly higher cutting speeds, the achieved total SCL during the turning tests on the case-hardening steel were significantly higher than for Alloy 718. Similarly, the cutting forces were significantly lower for the case-hardening steel as compared with Alloy 718 for the tested conditions. These effects are to a large extent likely to be caused by different thermo-mechanical properties of the machined materials (see chapter 4). However, despite the impact of thermo-mechanical properties, the influence of microstructural constituents on the tool wear can also play a role on the flank wear. Such a behavior is particularly likely when comparing the tests conducted on workpieces of the same material type, i.e. the two superalloys (Fig. 17d) and the two stainless steel workpieces (Fig. 17c). In both cases significantly varying flank wear was observed even though the thermo-mechanical properties and resulting cutting forces were in the same ranges when comparing the two superalloys or the two stainless steel workpieces.

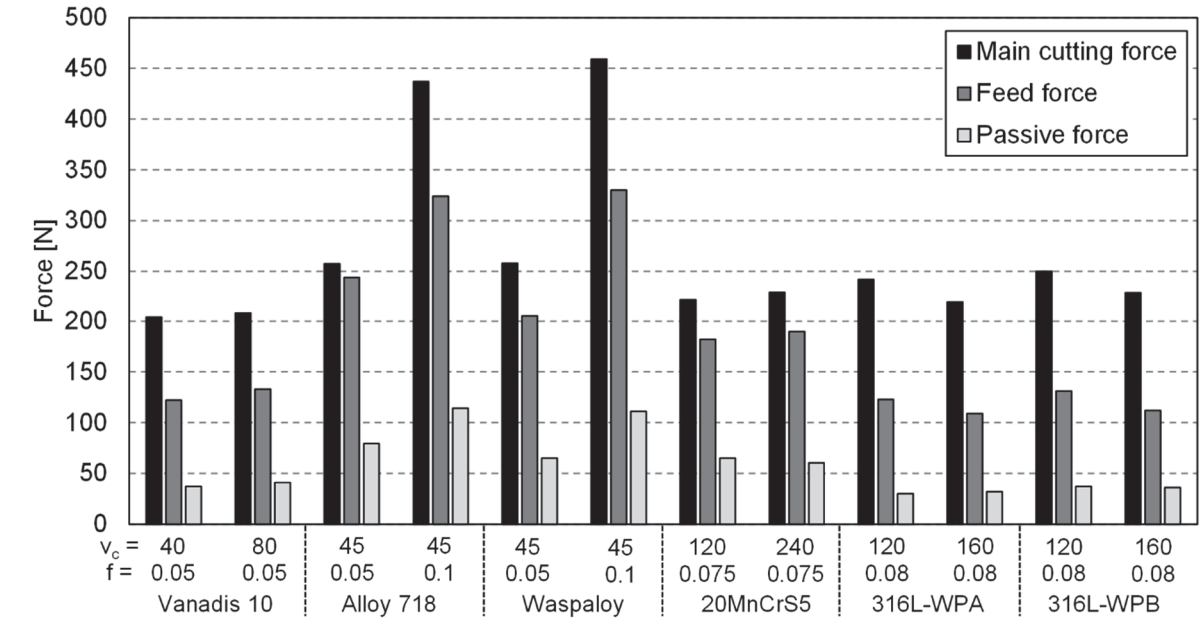

Fig. 18: Summary of measured force components acting on the inserts during turning tests on the different steel workpieces and the superalloys (Alloy 718 and Waspaloy) using uncoated tools. The two 316L stainless steel workpieces are denoted as "WPA" and "WPB". All forces were measured during the beginning of cut, i.e. when the cutting tools were still unworn.

6.3 Characterization of tool wear and determination of underlying wear mechanisms

The described characteristic properties and microstructures of the different workpiece material types (see section 6.1) should result in different wear patterns on the worn tool surfaces. The present section is devoted to comparing the microscopic wear features resulting from machining the different types of workpiece materials. The shown SEM micrographs and EBSD misorientation maps were obtained at about the center of the flank wear land on the major cutting edge, i.e. at around half the depth of cut. Furthermore, the mechanisms responsible for the wear are discussed.

After the turning tests the worn tools were characterized across different length scales, primarily by use of SEM in combination with associated techniques. Initially, some overview micrographs of worn, uncoated cutting edges are summarized in Fig. 19. All investigated cutting inserts had layers of workpiece material adhered to the worn tool surface on flank and rake face. The tendency of material adhesion was most pronounced in case of machining the 316L stainless steel (example shown in Fig. 19b), where the entire flank wear land and chip contact zone are covered by workpiece material. Comparably less adhesion was seen in case of machining the Vanadis 10 tool steel where parts of the worn tool surfaces appear almost free of adhered layers revealing the underlying WC grains (see bright zones in Fig. 19a). It should however be noted that even such seemingly adhesion-free zones often exhibited very thin adhesion layers. Detection of such thin layers usually required higher magnification and lower acceleration voltages (5 kV or lower).

However, no clear indications regarding the active wear mechanisms during cutting the different workpiece material types can be seen in the overview micrographs in Fig. 19. In an effort to make distinctions between the different active tool wear mechanisms, the following subsections contain a summary of electron microscopy studies on worn flank surfaces after machining the different workpiece material types.

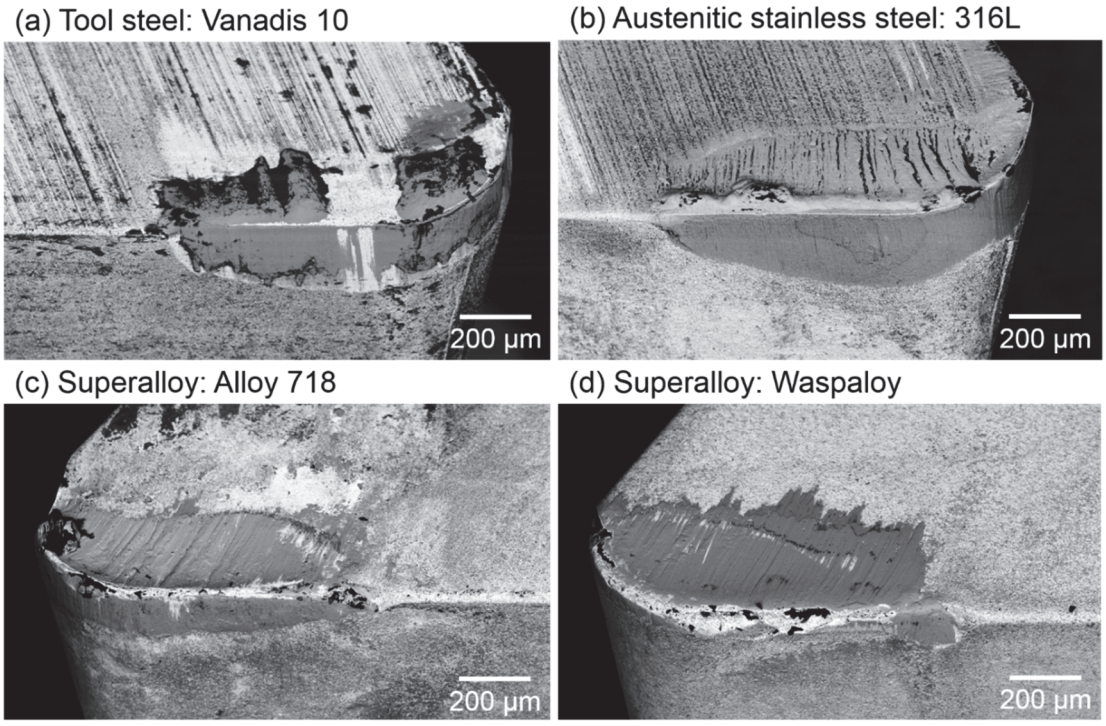

Fig. 19: SEM micrographs (12 kV acceleration voltage) of uncoated tools after the machining tests. The cutting parameters were (a) v_c=80 m/min and f=0.05 mm/rev; (b) v_c=160 m/min and f=0.08 mm/rev; (c), (d) v_c=45 m/min and f=0.1 mm/rev. The tool in (b) was used for cutting Workpiece A. The depth of cut was 1 mm for all tests.

6.3.1 Microscopic features of primarily abrasion- and dissolution-induced tool wear

As discussed earlier, tool wear mechanisms such as abrasion, diffusion/dissolution, adhesion, or plastic deformation can be active simultaneously during machining. This overlap of different mechanisms makes their identification challenging. It is therefore important to know the microscopic wear-features which are characteristic for an individual tool wear mechanism. This subsection is focused on providing such knowledge in case of abrasion- and dissolution-induced tool wear of uncoated cemented carbide inserts by focusing on the tests conducted on the Vanadis 10 and 316L workpieces. These tests were conducted specifically for the purpose of obtaining primarily abrasive tool wear and tool wear caused primarily by dissolution.

Theoretical considerations of abrasive and dissolution tool wear

Whether a particle within a workpiece can cause abrasion of the tool material when it comes into contact with the tool during cutting depends largely on the particle's hardness relative to the tool material at the respective temperatures. The machined workpiece materials contained different types and amounts of potentially abrasive particles (see Fig. 16). In Fig. 20, a summary of the ranges of reported high-temperature hardness of the majority of the relevant workpiece-particles is provided. The hardness range of WC, the main constituent of the uncoated cemented carbide tools, is displayed for comparison.

Depending on its source, the reported hardness data can vary substantially. It is likely that these variations have (to some extent) to do with differences in the experimental details during hardness measurements but are mainly related to variations in the stoichiometry, grain size, and porosity of the investigated compounds. For example, the hardness variations of the $(Fe,Cr)_7C_3$ carbide and cementite ($(Fe,Cr)_3C$) are related to different Fe/Cr ratios [68].

Of the investigated material types, Vanadis 10 and 316L exhibited the most significant differences regarding the amount of hard, abrasive phases in their microstructures. This can be seen in Table 8 and the respective micrographs in Fig. 16. The carbides in the Vanadis 10 workpiece can act as abrasive particles, this is because the hardness range of MC carbides (vanadium-rich) and M_7C_3 carbides (iron- and chromium-rich) lies above the range of WC (see Fig. 20a). The abrasive potential and the high fraction of the carbides (in total nearly 24 vol%) suggest abrasion to be the main wear mechanism of the present cemented carbide tools when machining the tool steel.

In contrast, the sulfide inclusions of the 316L workpiece are significantly softer than the WC grains (see Fig. 20a), they are therefore not able to contribute to tool wear by abrasion. Oxide inclusions in 316L steel can –depending on exact stoichiometry– potentially have high enough hardness to cause abrasive tool wear. Due to the relatively small quantity of oxide inclusions in the investigated 316L workpiece (around 0.04 vol%) and the fact that the material was calcium-treated to obtain comparably soft oxide inclusions, their overall abrasive effect is expected to be of minor importance. Abrasive tool wear should therefore not play a significant role when machining this 316L workpiece using uncoated cemented tungsten carbide tools.

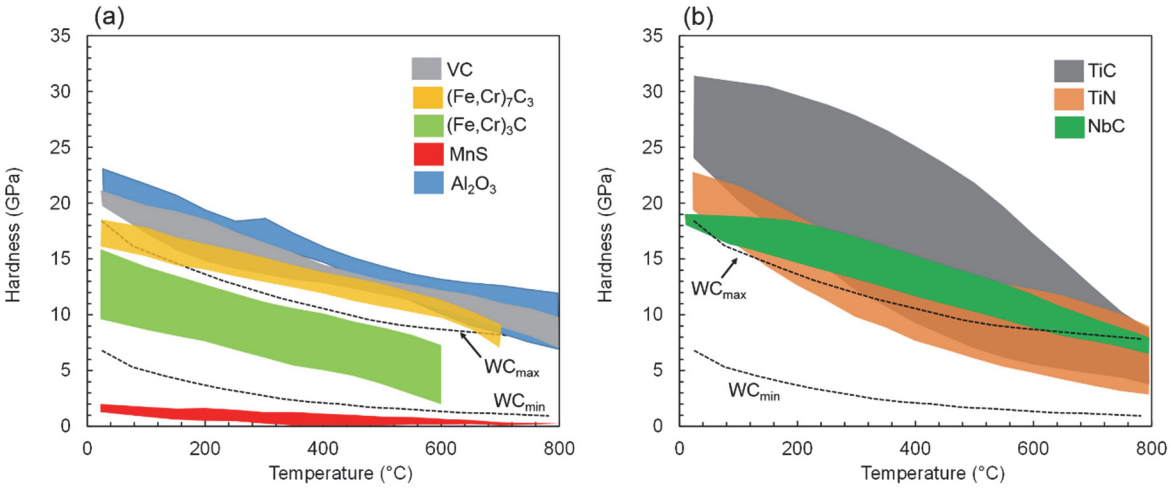

Fig. 20: Ranges of reported high-temperature hardness data of particles present in (a) the investigated steel workpieces and in (b) the superalloy workpieces: VC [69], [70]*; $(Fe,Cr)_7C_3$* [68]*; $(Fe,Cr)_3C$* [68], [71]*; MnS* [72]*; Al_2O_3* [73], [74]*; TiC* [69], [70], [75], [76]*; TiN* [77], [78]*; NbC* [75], [79], [80]. *For comparison, the hardness range of WC is presented as dashed lines* [18], [75], [81].

Table 8: Results of quantification of different particles present in the Vanadis 10 tool steel and the 316L austenitic stainless steel.

Workpiece material	Particle type	Content [vol%]	Average size [µm²]
Vanadis 10	MC carbide	16.2	1.1
	M_7C_3 carbide	7.4	3.1
316L (Workpiece A)	MnS	0.13	5.3
	Oxide inclusions	0.04	2.6

Another possible active mechanism is dissolution/diffusion of tool constituents into the chip/workpiece (see section 3.3). Calculated solubilities of different tool constituents in pure ferritic and austenitic iron are provided in Fig. 21a to c.

Evidently, WC has the highest solubility, i.e. lowest resistance against dissolution, for machining both ferritic and austenitic iron (Fig. 21a). In comparison, common coating materials such as TiC, TiN, and Al_2O_3 should have significantly higher resistance against wear by dissolution. This can be deduced from the fact that their solubilities in ferrite and austenite lie several orders of magnitude below WC (compare Fig. 21).

For uncoated tools, it should also be highlighted that below 1200 K the solubility of WC in austenitic iron is expected to be about two orders of magnitude higher than in ferritic iron (see Fig. 21a). This suggests that for similar ranges of process temperatures, dissolution wear of WC is more pronounced in case of machining the austenitic 316L workpiece as compared with the ferritic Vanadis 10 material.

In summary, the discussion regarding the hardness and solubility data presented in Fig. 20 and Fig. 21 lead to the conclusion that for uncoated tools, abrasion is expected to be dominant when machining the Vanadis 10 tool steel while no significant abrasion should occur in case of the 316L austenitic stainless steel. Machining 316L with uncoated tools should instead primarily lead to tool wear by dissolution.

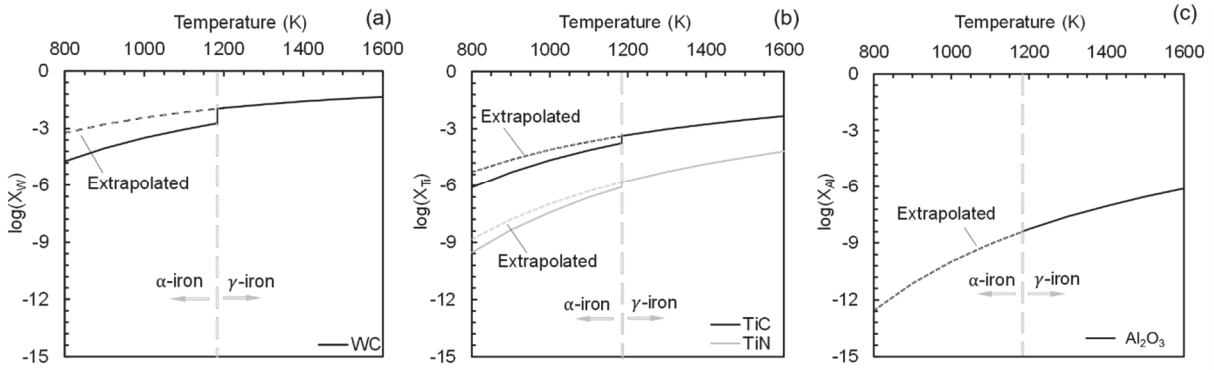

Fig. 21: Comparison between (a) WC and (b,c) commonly applied coating materials regarding their estimated solubility (in mole fraction X) in pure iron (α-iron: ferrite, γ-iron: austenite) as a function of temperature [82].

Characterization of worn, uncoated tool flank surfaces

The following paragraphs contain a summary of the SEM-based examination of abrasive- and dissolution-dominated tool wear when machining the tool steel and austenitic steel, respectively.

The two investigated tool wear mechanisms resulted in significantly different topographies of the worn WC grains. As seen in Fig. 22a, abrasive wear in case of machining the tool steel resulted in WC grain surfaces with sub-micron sized grooves which are aligned parallel to the sliding direction of the workpiece/chip on the flank/rake side of the inserts. The observed grooves are smaller than the average size of the carbides present in the workpiece. This is likely because of the carbides breaking up into smaller fragments during sliding contact with the tool surfaces. Additionally, some WC grains are subjected to micro-fragmentation (see Fig. 22a).

In contrast, mainly dissolution-wear during machining the 316L stainless steel bars led to flat-worn and smooth WC grain surfaces (Fig. 22b). Neither grooves aligned with the workpiece sliding direction, nor micro-fragmented WC grains were seen. This wear-topography was characteristic for adhesion-free WC grains after machining both 316L workpieces using 120 m/min and 160 m/min cutting speeds.

Similarly to the topography, significant differences between machining both materials were observed regarding the induced surface-deformation on the tools' flank faces (see EBSD results in Fig. 22c and d). The WC grain surfaces in case of machining Vanadis 10 were deformed during cutting. This can be seen by the measured strain, i.e. the mainly green and yellow pixels (2-3° misorientation) in the local misorientation map of Fig. 22c. No significant local misorientation and hence strain was measured after machining the stainless steel. The corresponding EBSD map in Fig. 22d shows mostly blue pixels, i.e. close to 0° local misorientation.

The wear topography and surface-deformation were also examined for the higher cutting speeds used for the two workpiece materials. In both cases, no significant differences were observed when comparing the results with the lower cutting speeds presented in Fig. 22.

Additional to the top-view examination, a cross section of an insert used for machining Vanadis 10 was examined using EBSD. Mapping of an area adjacent to the worn flank face showed that the strain within WC grains was confined to a narrow zone (< 1 μm deep) right beneath the worn flank surface. Plastic deformation of the tool material therefore occurred superficially and no bulk deformation of the WC phase in the tool had occurred.

The significantly different surface-characteristics of the worn tools after machining the 316L and Vanadis 10 workpieces are not likely to be the result of different loads acting on the tools during cutting. As seen in Fig. 18, similar feed and passive forces were measured during cutting both steels,

whereas slightly higher main cutting forces were seen in case of the stainless steel. The higher strain induced in the WC grain surfaces in case of Vanadis 10 are therefore expected to be a result of abrasion caused by sliding contact of the WC grains with the workpiece-carbides. In case of machining the 316L workpiece, no significant amounts of abrasive phases were present and therefore no abrasion and surface deformation of the tool took place during cutting.

The shown microscopic characteristics for abrasive- and dissolution induced tool wear in case of uncoated WC-Co tools can serve as a reference when investigating active wear mechanisms and other workpiece materials are machined (see upcoming subsection).

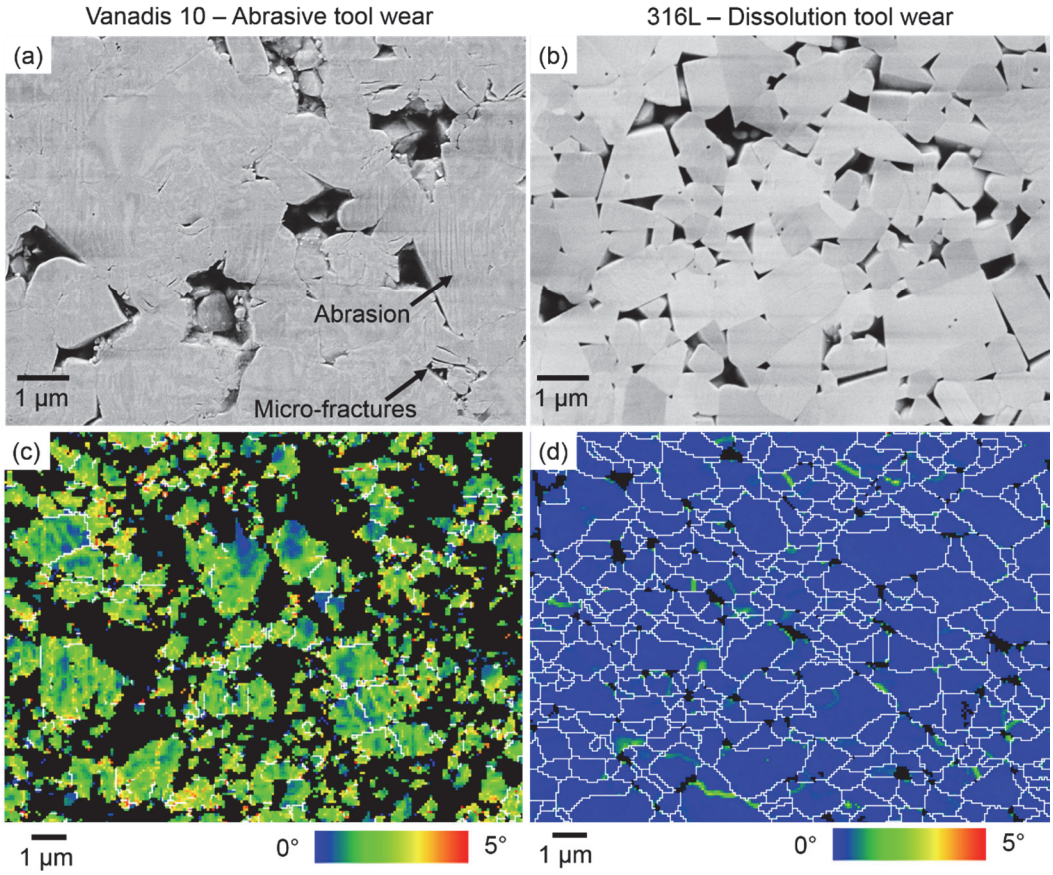

Fig. 22: Characteristics of worn WC grains on flank wear land after machining the Vanadis 10 tool steel and the austenitic stainless steel 316L: SE micrographs in (a) and (b); EBSD local misorientation maps in (c) and (d). Note that the EBSD maps do not show the same area as the SE micrographs. The tool steel was machined with v_c=40 m/min and f=0.05 mm/rev and the stainless steel was machined with v_c=120 m/min and f=0.08 mm/rev. The depth of cut was 1 mm in both cases. The presented results were obtained after removal of adhered workpiece material by etching.

6.3.2 Flank wear mechanisms for machining the superalloys and case hardening steel

The appearance of the flank wear topographies and the presence of surface deformation after machining the superalloys (see Fig. 23a and c) and its resemblance to the characteristics of abrasive tool wear presented in subsection 6.3.1 suggest that abrasive wear was a major active mechanism when machining the superalloys. Note that the shown micrographs in Fig. 23a and c are characteristic for machining both superalloy workpieces (Alloy 718 and Waspaloy).

As seen in Fig. 23b and d, machining the case hardening steel yielded in smooth surfaces of most of the worn WC grains with occasional presence of grooves and nearly strain-free WC grain surfaces. These features are most similar to the characteristics of dissolution wear shown in Fig. 22 (smooth, strain-free surfaces) with only minor signs of abrasive wear (grooves, ridges).

Based on the microscopic wear characteristics, it is therefore suggested that the contribution of abrasion to the tool wear is larger in case of machining Alloy 718 and Waspaloy than when machining the case-hardening steel. Tool wear in case of the steel is consequently expected to be mainly caused by dissolution wear with minor contributions of abrasion.

The possible reasons for the difference in the contribution of abrasion to the overall wear rate for both material-types can be explained by looking at the microstructures of the machined materials: from the metallographic examinations done on the workpieces (see example micrographs in Fig. 16), it could be seen that all three alloys contain potentially abrasive phases. In case of the superalloys these are primary carbides and TiN inclusions, in total about 0.36 vol% and 0.07 vol% for Alloy 718 and Waspaloy, respectively. Both particle types have sufficiently high hardness to abrade the tool material (see Fig. 20b). For the steel on the other hand, cementite and mainly Al-rich oxides (likely Al_2O_3) were identified. Al_2O_3 has sufficiently high hardness to act as abrasive particles but their quantity was only about 0.01 vol%. Despite its comparably high content of around 5.6 vol%, the abrasive potential of cementite is comparably low due to its lower hardness compared to the other phases in the steel and superalloys (compare Fig. 20a and b). Based on this discussion, the microstructural constituents in the superalloys have a higher abrasive potential which can help explain the higher contribution of this wear mechanism as compared with machining the case-hardening steel.

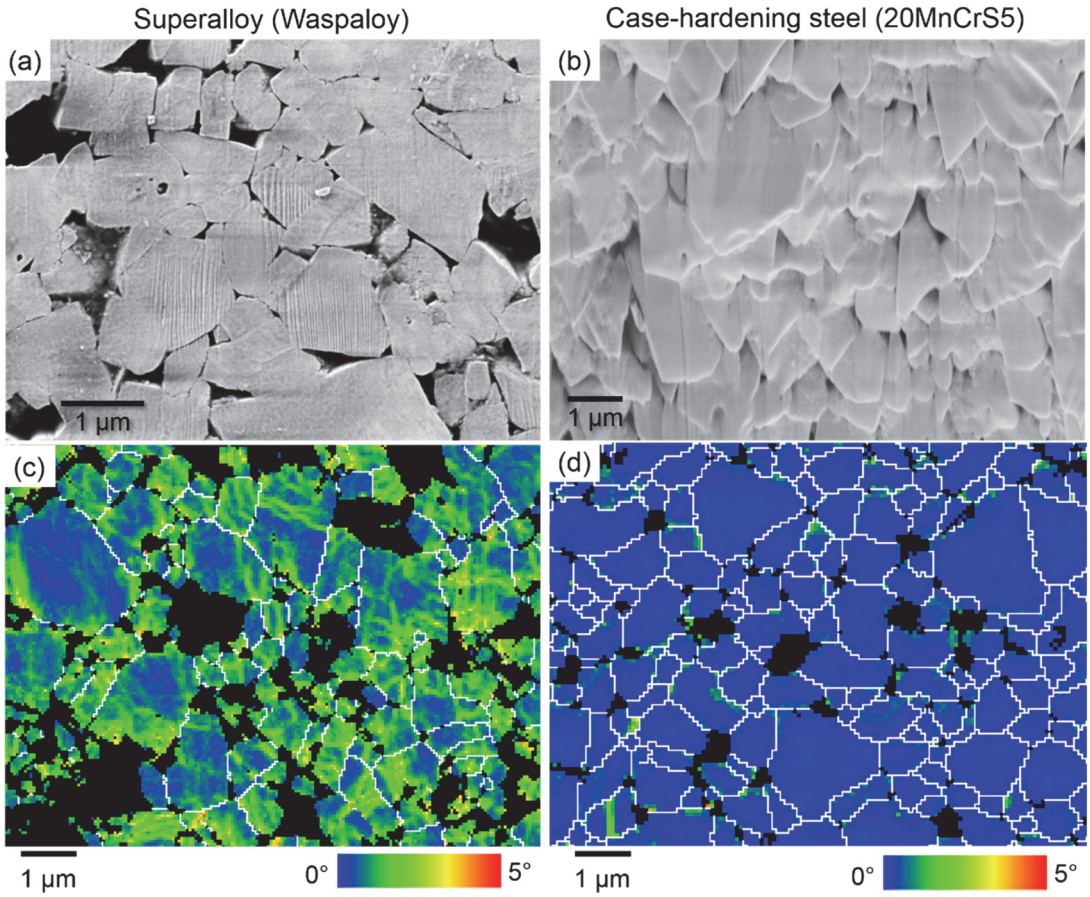

Fig. 23: Characteristics of worn WC grains on flank wear land after machining the investigated superalloys and the case-hardening steel: SE micrographs in (a) and (b); EBSD local misorientation maps in (c) and (d). Note that the EBSD maps do not show the same area as the SE micrographs. The Waspaloy workpiece was machined with 45 m/min cutting speed and 0.05 mm/rev feed rate and the case-hardening steel with 240 m/min cutting speed and 0.075 mm/rev feed rate. The depth of cut was 1 mm in both cases. The presented results were obtained after removal of adhered workpiece material by etching.

6.4 Influence of workpiece material microstructure on wear characteristics

After identifying the probable active flank wear mechanisms for machining the different types of workpiece materials in the preceding section, this section is focused on the influence of workpiece-microstructure on the overall flank wear in case of the two superalloys and the two bars of 316L stainless steel.

6.4.1 Comparison of Alloy 718 and Waspaloy

The tool life test results presented in Fig. 17 revealed an interesting discrepancy in flank wear development when machining the two superalloys. Under both test conditions, Alloy 718 led to significantly faster progression of flank wear as compared with machining Waspaloy. The same trend has been reported previously under conventional cooling conditions [66] and under influence of high-pressure coolant supply [67]. The present subsection is devoted to discussing the possible reasons for the differences in wear development during turning.

A comparison of the cutting forces associated with machining the two superalloy workpieces does not provide the answer for the different wear rates. Even though the investigated Alloy 718 workpiece was about 13 % harder than the Waspaloy workpiece (see Table 7), similar cutting forces

were measured when cutting both materials with identical cutting parameters (see Fig. 18). For both tested alloys, the main cutting forces were around 250 and 450 N for the low and high feed rate, respectively. Regarding the feed forces, a difference was obtained for the lower feed rate where around 250 and 210 N were measured for Alloy 718 and Waspaloy, respectively. For the higher feed rate, however, the feed forces were similar and at around 325 N. Consequently, it is unlikely that differences regarding mechanical loads acting on the cutting tools are responsible for the different flank wear behavior during cutting the two alloys.

As discussed in chapter 4, the thermal properties of a workpiece influence the temperature in the cutting zone. Table 9 contains a comparison of the thermal properties of Alloy 718 and Waspaloy. Accordingly, their thermal conductivities and specific heat capacities lie in similar ranges. The dissipation of heat from the cutting zone into the chip/workpiece is therefore likely to be similar during machining both alloys. The specific heat capacities reported for elevated temperature indicate that slightly more energy is required to raise the temperature of Alloy 718 as compared with Waspaloy. Consequently, for the same cutting parameters, similar amount of tool wear, and similar cutting forces, slightly lower cutting temperatures could occur when machining Alloy 718 as compared with Waspaloy.

Similarly to the mechanical loads, it is unlikely that significantly different thermal loads during cutting the two alloys cause the large variation in flank wear. This is because slightly lower temperatures in the cutting zone when machining Alloy 718 would suggest lower tool wear, mainly due to less pronounced thermal-softening of the tool material. However, the opposite trend of Alloy 718 being associated with faster progression of flank wear was observed during the tests (see Fig. 17d).

Table 9: Comparison of thermal properties of Alloy 718 and Waspaloy at different temperatures [83], [84].

Property	Material	21 °C	538 °C	871 °C
Specific heat capacity [J/(kgK)]	Alloy 718	430	560	645
	Waspaloy	-	540	580
Thermal conductivity [W/(mK)]	Alloy 718	11.4	19.6	24.9
	Waspaloy	10.7	18.1	24.1

In order to investigate whether differences in tool wear by dissolution during cutting could have contributed to the overall flank wear differences between Alloy 718 and Waspaloy, diffusion couple tests were conducted. The goal of the tests was to compare the contribution of diffusion/dissolution processes to the wear of uncoated cemented carbide inserts when machining the two alloys. The investigation comprised of diffusion couple tests which enabled to simulate the intimate tool/workpiece contact in the cutting zone under static, controlled conditions. It should be noted that the static test conditions are different from the dynamic situation at the interface of tool- and workpiece-material in the cutting zone. However, such static diffusion couple tests can provide a qualitative comparison of the dissolution wear when machining both superalloys.

Fig. 24 depicts EDS line scans across the interfaces of the tested diffusion couples. In all graphs, a steep decrease or increase of the X-ray signal originating from W and Ni can be seen across the tool/superalloy interfaces (the interface is approximately at the center of the x-axis). A slightly more shallow decrease or decay of the X-ray intensities can be seen for the diffusion couples tested at 1000 °C. This is because diffusion is a thermally activated process and hence more interdiffusion between the tool and the superalloys occurs at higher test-temperatures. However, when comparing the Alloy 718- and Waspaloy-containing diffusion couples tested at the same temperature, no

distinct difference can be observed regarding the size of the diffusion-affected zones adjacent to the tool/workpiece interface (see EDS line scans in Fig. 24).

Even though wear by dissolution is likely active with a potentially significant contribution to the tool wear when cutting both workpiece materials, the presented experimental results suggest that it is unlikely that varying magnitudes of dissolution of tool atoms into the chip or workpiece are a major factor contributing to the differing flank wear developments when machining the two alloys with uncoated cemented carbide inserts.

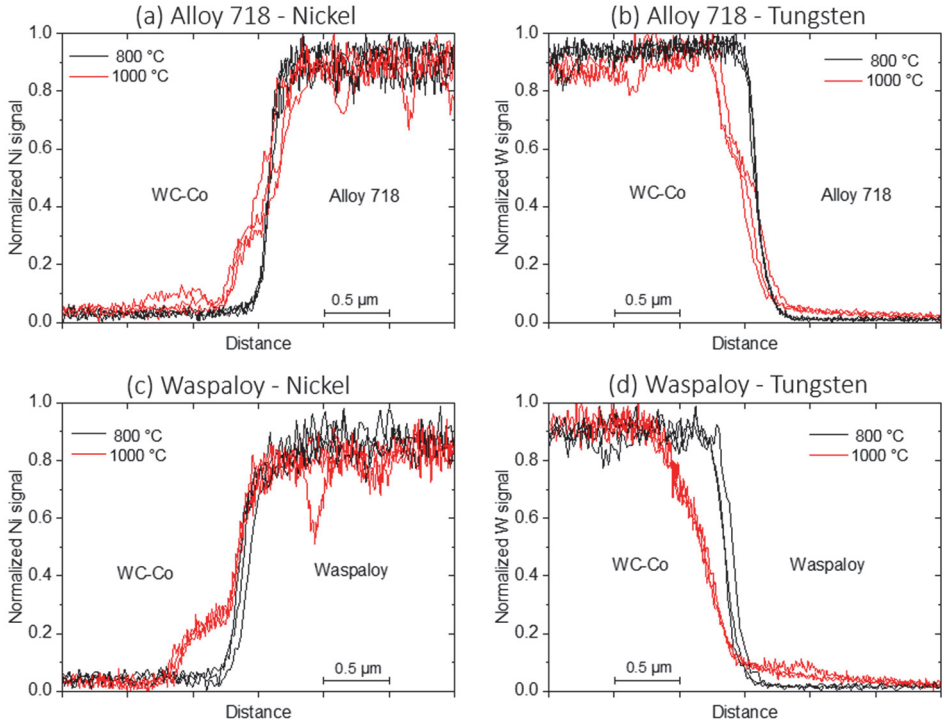

Fig. 24: Qualitative comparison of EDS line scans across the interfaces of the tool material (WC-Co) and superalloys after static diffusion couple testing for 90 min at 800 °C and 1000 °C, respectively.

When comparing the microscopic characteristics of worn tool surfaces after machining both alloys, no significant differences regarding the wear topographies could be seen. In both cases, worn WC grains exhibited characteristics similar to the ones exemplified in Fig. 23a. As discussed previously, and based on the microscopic wear-features, abrasive wear is expected to be a significant contributor to flank wear during cutting both alloys.

A more detailed examination and quantification of hard, potentially abrasive phases in both alloys was therefore conducted. Table 10 presents a summary of the obtained results. Quantification of primary carbides and non-metallic inclusions in both workpieces showed that Alloy 718 contained significantly higher fractions of these phases as compared with Waspaloy. It is therefore likely that abrasive wear was more pronounced in case of machining Alloy 718 which in turn explains why flank wear develops faster when machining this alloy.

Table 10: Quantities of hard, abrasive phases in the investigated superalloy workpieces. Primary carbides (NbC and TiC) and non-metallic inclusions (TiN). The total investigated sample area was about 15.5 mm² for each alloy. [85]

	Alloy 718		Waspaloy
Type of particles	TiN	NbC	TiC and TiN
Average number of particles per mm²	14.2	133.8	22.5
Area fraction [%]	0.05	0.31	0.07
Median of particle projection area [µm²]	24.8	14.8	12.4

6.4.2 Batch-to-batch variations in 316L austenitic stainless steel

This subsection deals with the reasons behind the observed differences in flank wear development when machining the two 316L austenitic stainless steel workpieces. As seen in Fig. 17, the turning tests revealed significant differences in the flank wear developments when machining the two workpieces supplied by different manufacturers. While a steady increase of tool flank wear was observed for machining the workpiece of supplier A, the flank wear stayed nearly constant throughout the entire test in case of supplier B's workpiece. A summary of the conducted metallographic investigation on both workpieces is provided in Table 11. The difference in grain size between both workpieces of the present study (see Table 11) is expected to mainly influence the tool notch wear behavior when cutting the two workpieces (see chapter 4). As reported by e.g. Jiang et al. [46], austenite grain size has only an insignificant influence on flank wear when machining stainless steel.

Table 11: Summary of the comparative metallographic study conducted on the two 316L austenitic stainless steel workpieces. The presented values were obtained on samples extracted from the outer diameter of the steel bars which is the part which was utilized for the machining tests.

	316L workpiece	
	Supplier A	Supplier B
Grain size, mean lineal intercept length [µm]	33 ± 2	43 ± 5
Hardness [HV]	154 ± 14	180 ± 2
Hardness [GPa]	1.51 ± 0.14	1.77 ± 0.05
Delta ferrite (vol%)	Insignificant	0.07 ± 0.09
Sulfide inclusions (vol%)	0.13	0.11
Oxide inclusions (vol%)	0.04	0.01

Differences in hardness cannot explain the variations in flank wear development either: as seen in Table 11, the workpiece of supplier B was about 17% harder than the material of supplier A. This is in line with the cutting force measurements showing slightly higher force components when cutting Workpiece B (see Fig. 18). Higher hardness and resulting cutting forces would suggest slightly higher thermo-mechanical tool-loads which in turn would lead to faster wear when machining workpiece B, however the opposite was observed during the turning tests.

Instead, the micro-constituents present in the workpieces are likely the tool-life limiting factor in this case. Both workpieces contained different types of non-metallic inclusions and stringers of delta ferrite. Regarding the latter and in light of the previously presented data on solubility of WC

in austenite and ferrite (higher solubility and hence dissolution-wear for machining austenite, see Fig. 21a), the workpiece containing more delta ferrite should be subjected to less wear by dissolution. Examination of metallographic samples of the machined sections showed that only the material of supplier B contained significant amounts of delta ferrite (see Table 11). However, since the amount of delta ferrite was very low, this effect is expected to be only of minor significance.

Characterization of worn tools after machining showed that machining the two workpieces has promoted the formation of different types of adhesion layers on the worn tool flank surfaces after machining the two workpieces. A series of SEM images of an insert after machining workpiece B is provided in Fig. 25. An oxygen-rich transfer layer was found to cover large parts of the flank wear land (see Fig. 25b to d). This layer was located in the lower part of the flank wear land including the transition from the worn to unworn tool surface and it remained on the surface even after etching of the tool for removal of adhered material. The adhesion-free, worn WC grains (upper half of micrograph in Fig. 25d) showed the same topographical features which were shown to be characteristic for tool wear by dissolution discussed in subsection 6.3.1. In case of machining workpiece A, no such oxygen-rich transfer layer could be found, neither before nor after etching the insert for removal of adhered material.

Given the reported effects of non-metallic inclusions on the wear of metal cutting tools by e.g. formation of stable, protective layers [47]–[51], it is likely that different types of inclusions present in the workpieces are responsible for the different mechanisms at the tool/workpiece interface during cutting. It is suggested that the layer which has exclusively formed during machining of workpiece B provided protection against dissolution-wear by forming a passivating film on the tool surface and thereby limited the overall flank wear during cutting this workpiece. During machining of the other workpiece, no such layers have formed and hence the tools were not protected against dissolution-wear which explains the higher flank wear rate.

A closer examination of the inclusions in both workpieces showed that both workpieces contained similar quantities of sulfide inclusions (see Table 11). EDS analysis suggests that the sulfides in both workpieces were MnS containing small amounts of chromium. As discussed in subsection 6.3.1, sulfide inclusions are very soft and are generally assumed to have beneficial influence on the tribological conditions at the tool/workpiece interface in the cutting zone [50]. However, they usually do not contribute to the formation of stable, protective films on tool surfaces [86].

As opposed to the sulfide inclusions, closer examination of the oxide inclusions revealed compositional differences between both workpieces. The analyzed oxide inclusions could be divided into four distinct groups. Each group's average composition is summarized in Table 12.

According to Nordgren and Melander [86], the mechanical properties and the resulting deformation behavior are the decisive factor for the ability of inclusions to form stable, protective layers on tool surfaces. As for example shown in the comprehensive work by Kiessling and Lange [87]–[90], the mechanical properties of oxide inclusions can vary significantly depending on their exact composition. It can therefore be expected that the four groups of oxide inclusions (Table 12) exhibit varying mechanical properties which will affect their abilities to form protective layers on the tools during cutting. It seems that the specific composition of the inclusions in workpiece B are favorable for the formation of protective layers on uncoated cemented tungsten carbide tools for the tested cutting conditions.

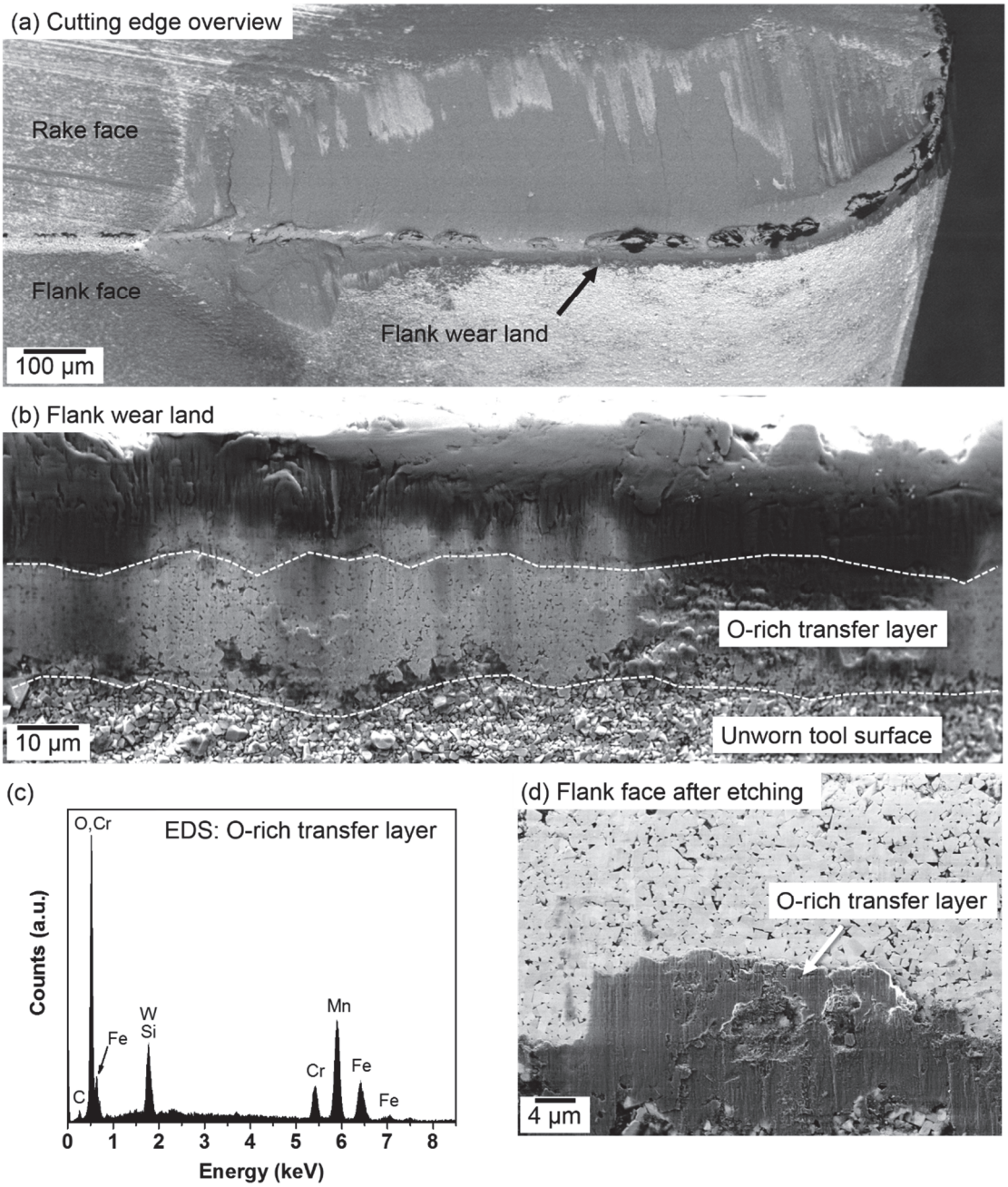

Fig. 25: Worn cutting tool after machining the 316L workpiece from supplier B using 160 m/min cutting speed. (a) overview micrograph; (b) closer view of flank wear land with partly electron-transparent transfer layer using 20 kV acceleration voltage; (c) EDS spectrum obtained on O-rich adhesion layer; (d) micrograph (5 kV acceleration voltage) of same tool after removal of adhered workpiece material.

Table 12: Average composition (in at%) of different types of oxides in both investigated 316L workpieces. Standard deviations are given in brackets. The composition of each inclusion-type was measured on at least 5 inclusions using EDS point analysis (15 kV acceleration voltage of primary electron beam). [91]

Work-piece	Element							
	O	Si	Ca	Al	Mn	Ti	Mg	Cr
A	57.3 (± 1.9)	-	-	8.8 (± 0.5)	15.0 (±0.5)	-	-	18.9 (±1.9)
B	66.6 (±1.4)	-	-	-	-	27.4 (± 3.2)	-	6.0 (±2.2)
A	59.1 (± 0.8)	15.5 (± 0.4)	9.4 (± 0.6)	6.3 (± 0.6)	6.4 (± 0.9)	-	0.7 (± 0.1)	0.9 (± 0.4)
B	63.4 (± 0.9)	10.8 (± 0.4)	12.4 (± 0.8)	4.7 (± 0.2)	3.7 (± 0.7)	1.8 (± 0.5)	1.6 (± 0.3)	0.8 (± 0.2)

6.5 Flank wear mechanisms when using coated tools

As a complement to the uncoated tools, some tests with coated tools were conducted. This was done for the tool steel and stainless steel. The results in this section exemplify that the active/dominant tool wear mechanisms are also dependent on the employed tool/coating material and can change when e.g. adding coatings to the cutting tools. Additionally, the increased complexity of the wear-characterization of coated tools is highlighted.

From theoretical considerations and the observed wear features on the cutting tools (subsection 6.3.1) it was concluded that the uncoated cemented carbide tools wear by mainly abrasion and dissolution when machining the tool steel and stainless steel, respectively. The corresponding wear features after machining these two materials with TiCN-Al_2O_3 coated tools are summarized in Fig. 26.

In case of machining the tool steel, the topographies of the worn Al_2O_3 and TiCN coatings (see Fig. 26b and c) are similar to the topography of WC grains of uncoated tools (compare Fig. 22a): the coating materials exhibit ridges and grooves which are aligned with the sliding direction of the workpiece during cutting. The presence of grooves is less pronounced in case of the TiCN coating. Based on these observations it is likely that –similar to the uncoated tools– abrasion is the main active mechanism responsible for the wear of the coating materials.

In contrast, the flank wear topography of the coating materials was significantly different from the uncoated tools when machining the 316L stainless steel. Despite the etching, some transfer material remained adhered to the tool surface locally (see Fig. 26e). The remaining transfer material complicates the assessment of the underlying, worn coating material. Nevertheless, it appears that the coating materials exhibit rougher surfaces as compared with the smooth, flat-worn tool constituents when using uncoated tools for machining this workpiece (compare with Fig. 22b). The high-magnified micrograph in Fig. 27 shows a small patch which is entirely free of adhered workpiece material. The TiCN surface exhibits a facetted fracture surface. Based on these observations and the fact that the solubility of the coating materials in iron are several orders of magnitude below the solubility of WC in iron (see Fig. 21) it is believed that tool wear by dissolution does not play a significant role for coated tools when machining the stainless steel. Instead, adhesion-induced localized chipping and micro-fragmentation of the coating is dominant for the wear of the TiCN and Al_2O_3 coatings when machining 316L under the investigated conditions.

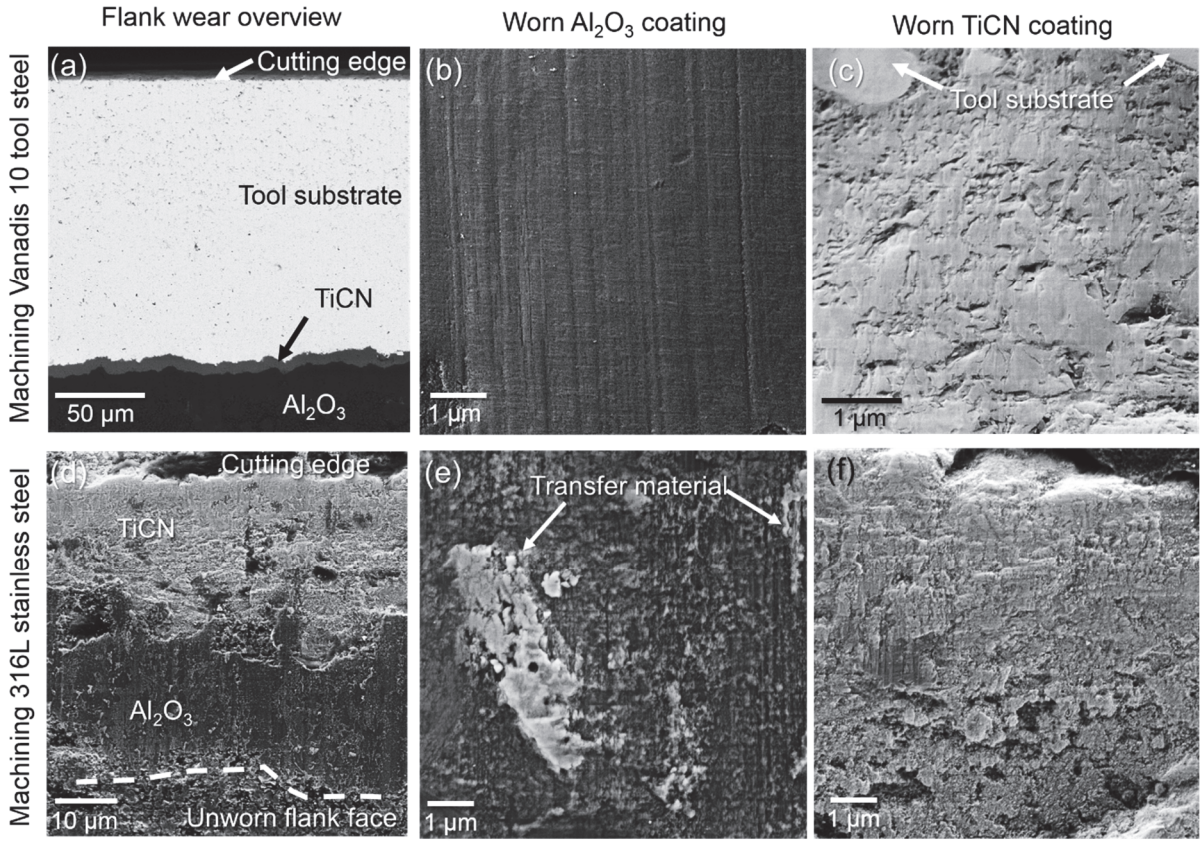

Fig. 26: Comparison of wear features on the flank surfaces of TiCN-Al_2O_3 coated cemented carbide tools after machining the tool steel and stainless steel. The tool steel was machined with v_c=80 m/min and f=0.05 mm/rev and the stainless steel was machined with v_c=160 m/min and f=0.08 mm/rev. The depth of cut was 1mm in both cases. The presented results were obtained after removal of adhered workpiece material by etching. [82]

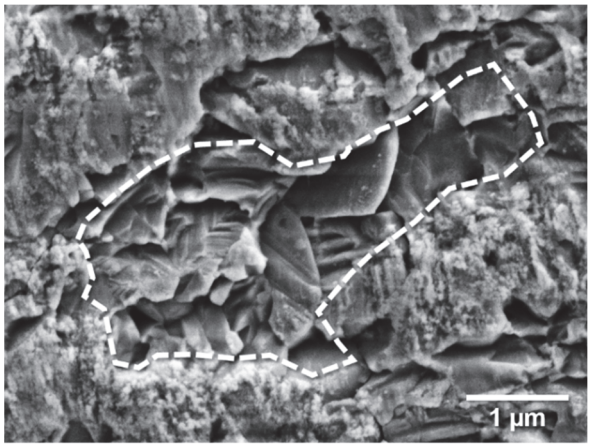

Fig. 27: Adhesion-free patch (encircled area) of worn TiCN coating surface after machining the stainless steel [82].

7 Conclusions

The main objective of the present work is to enhance the fundamental understanding of the influence of the workpiece material and its microstructure on flank wear of uncoated cemented carbide tools during metal cutting. In connection to the research questions (RQ) formulated in section 1.1, the following conclusions (summarized in Fig. 28) can be drawn:

Tool wear characteristics and underlying wear mechanisms during machining the investigated materials (RQ1 and RQ2)

- Investigations of the active wear mechanisms during metal cutting require in-depth analyses of the worn tool surfaces and of the microstructure of the machined workpieces.
- Results of these investigations in combination with available high-temperature hardness and solubility data of microstructural constituents in the workpieces help to better explain the characteristic flank wear behavior and microscopic wear-features on the tool surfaces after cutting the respective material.
- The high fraction of hard, abrasive carbides present in the **Vanadis 10 tool steel** leads to primarily abrasion-induced flank wear.
- Abrasive wear is a major contributor to the flank wear when machining the **superalloys Alloy 718 and Waspaloy**. Abrasion is mainly caused by primary carbides and non-metallic inclusions in the workpieces. Additionally, dissolution wear is likely to significantly contribute to the tool wear when machining these materials.
- Cutting the **case-hardening steel 20MnCrS5** with about 50% pearlite is dominated by tool wear by dissolution with minor contributions of abrasion. Mild abrasion is caused by cementite and small quantities of oxide and nitride inclusions in the workpiece.
- The very low amount of hard phases in its microstructure and comparably high solubility of the main tool constituent (WC) in **316L austenitic stainless steel** lead to tool wear by mainly dissolution.
- The microscopic features of **abrasive tool wear** on the cemented carbide tool material consisted of sub-micron sized groves combined with micro-fractured carbide grains. The worn tool surfaces are furthermore subjected to plastic deformation induced by the abrading particles of the workpiece sliding against the tool surface during cutting.
- **Wear by mainly dissolution** of the cemented carbide tool material results in smooth carbide surfaces. Neither grooves nor micro-fragmentation or plastic deformation of the carbide grains in the tool occur.

Microstructural differences and their influence and tool wear mechanisms and flank wear (RQ3)

- Using the same cutting parameters, turning **Alloy 718** resulted in up to ~180% higher maximum flank wear (at equivalent machining time) as compared with **Waspaloy**.
- Neither significant differences in tool wear by dissolution, nor differences in thermal and mechanical loads on the cutting tools during machining the two superalloys are major contributors to the different flank wear responses.
- Varying amounts of hard phases in the workpieces were responsible for the different flank wear rates. The total fraction of primary carbides and nitride inclusions was about 5 times larger for Alloy 718 which can explain the higher tool wear when machining this workpiece.

- Machining the same **austenitic stainless steel (316L)** with the same specifications but obtained from different suppliers can lead to very inconsistent flank wear rates. In the present case, around 80% less flank wear was observed for one supplier's workpiece at equivalent machining times.

- Readily available material data (e.g. grain size and hardness) cannot necessarily explain the resulting tool life for certain materials. For the investigated 316L workpieces these microstructural aspects could not explain the flank wear variations.
- The composition of non-metallic inclusions determines their behavior and role during contact with the tool surface in the cutting zone. The specific composition and resulting properties of the inclusions in one of the investigated workpieces led to build-up of a stable inclusion-layer. However, the composition of the other inclusions in the workpiece did not favor the formation of an inclusion-layer.
- If present, an inclusion layers can provide protection of the underlying tool material against further tool wear by limiting the dissolution of tool material into the chip/workpiece.

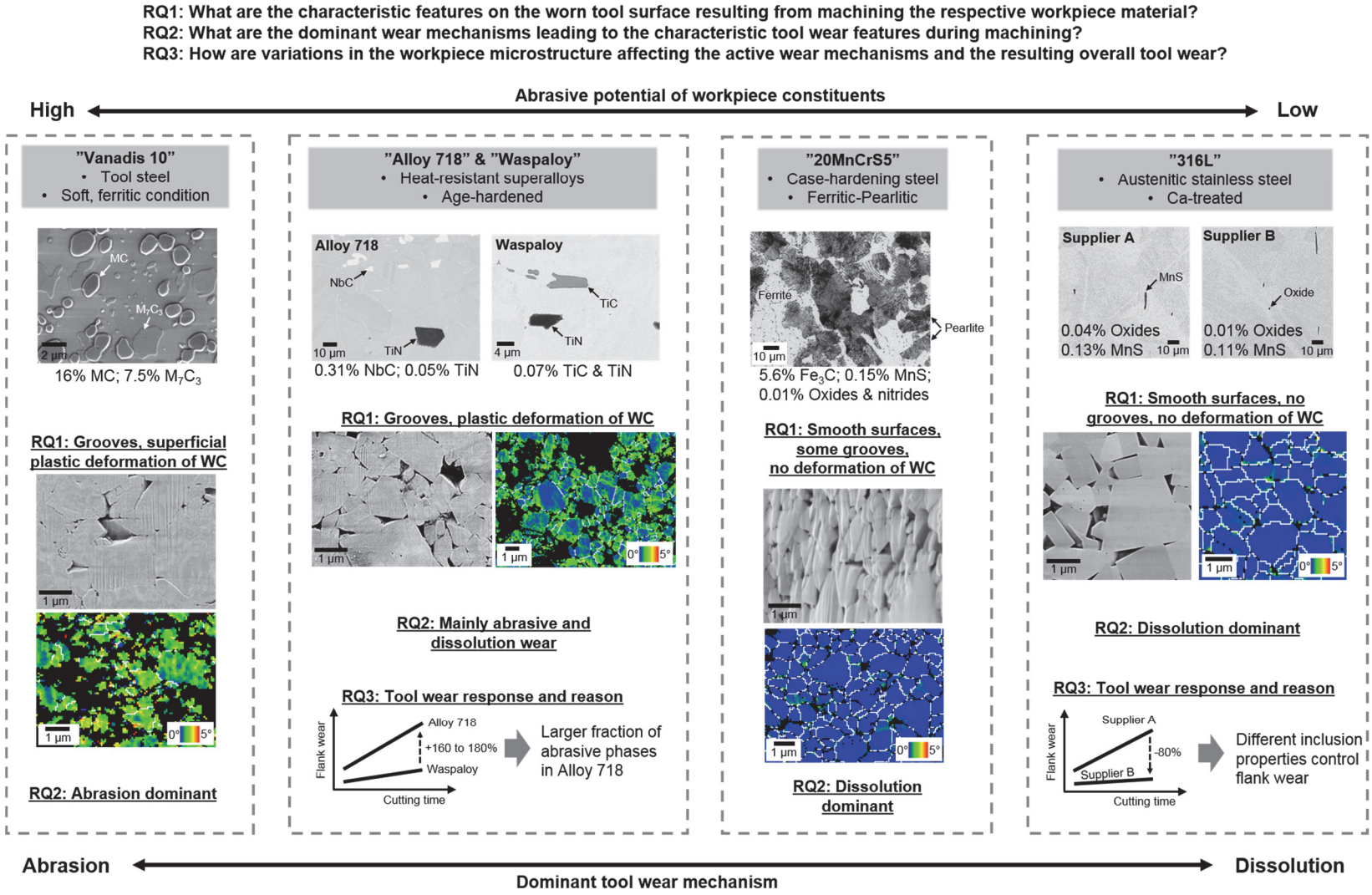

Fig. 28: Summary of main outcomes in relation to the research questions (RQs). Shown are the investigated workpieces with their characteristic microstructures and the resulting wear features on the flank surfaces. The horizontal arrangement is according to the respective dominating wear mechanisms using uncoated cemented carbide tools.

8 Future work

Based on the results presented in this thesis, the following suggestions are made regarding an extension of the work with respect to tool wear and the effect of the machined workpiece material.

- The present work was mainly focused on the tool wear occurring on the flank faces of the cutting tools. The presented characterization approach could be extended to study how the workpiece properties and microstructure can affect the wear on the rake side of the tool (e.g. depth of crater).
- The EBSD-based examination of the worn tool surfaces could be extended to study the effect of varying cutting parameters on the average strain induced during machining. In this way the effect of e.g. cutting speed (i.e. temperature in the cutting zone) on the relative contribution of abrasion and dissolution could be examined.
- The exact mechanisms and factors responsible for the ability of non-metallic inclusions present in the 316L workpieces are worth further examination. For this purpose, the initial phase of the build-up of the inclusion layer on the cutting tool and its evolution with increasing machining time should be examined. Complementary analysis with surface sensitive techniques (e.g. Auger electron spectroscopy and X-ray photoelectron spectroscopy) could provide additional information about the composition of the adhesion layer which could help explain the reason for its formation.
- During machining the two superalloys, Al-rich oxide layers were found to form on the tool surfaces during machining (see Paper III). An extended study, analyzing their exact role and potential influence on the tool wear would provide more insight whether this mechanism also contributes to the difference in flank wear when machining Alloy 718 and Waspaloy.

9 Acknowledgements

First and foremost I would like to thank my main supervisor and examiner Uta Klement for her help, guidance and encouragement during my time as a PhD student. Your door was always open for me and even during the busiest times you were providing me with all the necessary support. Thank you for that! I would also like to thank my co-supervisor Peter Krajnik for his invaluable input, guidance, and support. Thanks to you I also learned about the history of different manufacturing technologies and got to know about their early depictions in medieval books in my home city Nuremberg. Thanks are also extended to Tomas Beno (University West, Trollhättan) for the collaboration and support, in particular during the first half of my PhD.

Funding and support by Västra Götalandsregionen, the Chalmers Area of Advance - Production, the Chalmers Centre for Metal Cutting Research (MCR), and Vinnova are gratefully acknowledged. Furthermore, Chalmerska Forskningsfonden and Jernkontoret are thanked for providing financial support which enabled me to present our work at international conferences.

Furthermore I would like to acknowledge several people that I had the pleasure to work with:

- Amir Malakizadi for the enjoyable collaborations, interesting discussions, help with experiments, and for teaching me so much about metal cutting. Thank you!
- Nageswaran Tamil Alagan at University West in Trollhättan for the collaboration and especially for the nice time during our stay at the WoM conference 2019.
- Stefan Cedergren and Anders Wretland (both GKN aerospace) and Kumar Babu Surreddi (Dalarna University) for the collaboration and invaluable contributions to our work regarding machining of superalloys.
- Sven Friebe, Pietro Stuppa, and Mats Rudolf for their support and contributions during their thesis projects.
- Yiming Yao, Roger Sagdahl, Håkan Millqvist, Eric Tam, Peter Sotkovszki and Gustav Holmqvist for their support regarding various issues like microscopy, preparation of etchants, and cutting of (nearly) impossible-to-cut workpieces.
- Mats Norell for giving me the opportunity to act as the first assistant in his course "Materials characterisation and failure analysis". Even though it was a tough job at times, I enjoyed working with you and I learned a lot about a huge variety of materials and mechanical components.
- Simon Isakson and Dinesh Mallipeddi for the discussions about various topics including metal cutting and surface integrity.

A special thanks goes to Casey Jessop, Dmitri Riabov, Antonio Mulone, Sakari Tolvanen, Johanna Ekberg, William Hearn, and Camille Pauzon for the time we spent together during lunch breaks and outside work. I would furthermore like to thank all remaining former and current colleagues and friends at the Department of Industrial and Materials Science at Chalmers for making the last five years such an enjoyable and unforgettable time. Thanks for all the common activities like fika breaks, skiing in Norway, or curling on Hisingen.

Last but not least I want to thank my parents, my brother, my relatives, and friends in Germany for all their support and encouragement in the last years.

10 References

[1] R. W. Ivester *et al.*, "Assessment of machining models: progress report," *Mach. Sci. Technol.*, vol. 4, no. 3, pp. 511–538, 2000.

[2] H. K. Tönshoff, *Massivumformteile wirtschaftlich spanen*. Hagen, Germany: Industrieverband Massivumformung, 2010.

[3] P. Krajnik and F. Hashimoto, "Finishing," in *CIRP Encyclopedia of Production Engineering*, The International Academy for Production, Ed. Berlin, Heidelberg: Springer Berlin Heidelberg, 2018, pp. 1–9.

[4] F. Klocke *et al.*, "Technological and Economical Assessment of Alternative Process Chains for Blisk Manufacture," *Procedia CIRP*, vol. 35, no. February 2016, pp. 67–72, 2015.

[5] National Transportation Safety Board, "Aircraft Accident Report - Uncontained Engine Failure Delta Air Lines Flight 1288," Washington DC, USA, 1998.

[6] F. Klocke, *Manufacturing Processes 1*. Berlin, Heidelberg: Springer Berlin Heidelberg, 2011.

[7] F. W. Taylor, *On the art of cutting metals*. New York: The American Society of Mechanical Engineers, 1907.

[8] K. D. Bouzakis, N. Michailidis, G. Skordaris, E. Bouzakis, D. Biermann, and R. M'Saoubi, "Cutting with coated tools: Coating technologies, characterization methods and performance optimization," *CIRP Ann. - Manuf. Technol.*, vol. 61, no. 2, pp. 703–723, 2012.

[9] F. Pusavec, P. Krajnik, and J. Kopac, "Transitioning to sustainable production – Part I: application on machining technologies," *J. Clean. Prod.*, vol. 18, no. 2, pp. 174–184, Jan. 2010.

[10] F. Pusavec, D. Kramar, P. Krajnik, and J. Kopac, "Transitioning to sustainable production – part II: evaluation of sustainable machining technologies," *J. Clean. Prod.*, vol. 18, no. 12, pp. 1211–1221, Aug. 2010.

[11] DIN (the German Institute for Standardization), "DIN 8580 Manufacturing processes - Terms and definitions, division," 2003.

[12] S. Isakson, "Cryogenic Machining of Ti-6Al-4V Department of Industrial and Materials Science," Chalmers University of Technology, 2018.

[13] S. N. Melkote *et al.*, "Advances in material and friction data for modelling of metal machining," *CIRP Ann. - Manuf. Technol.*, vol. 66, no. 2, pp. 731–754, 2017.

[14] P. J. Arrazola, T. Özel, D. Umbrello, M. Davies, and I. S. Jawahir, "Recent advances in modelling of metal machining processes," *CIRP Ann.*, vol. 62, no. 2, pp. 695–718, Jan. 2013.

[15] M. Groppe, "Cemented Carbides," in *CIRP Encyclopedia of Production Engineering*, Berlin, Heidelberg: Springer Berlin Heidelberg, 2014, pp. 127–135.

[16] H. E. Exner, "Physical and chemical nature of cemented carbides," *Int. Met. Rev.*, vol. 24, no. 1, pp. 149–173, Jan. 1979.

[17] G. S. Upadhyaya, *Cemented tungsten carbides: production, properties, and testing*. Noyes Publications, 1998.

[18] J. E. Stahl, *Metal Cutting Theories and Models*. Lund, Sweden: Division of Production and Materials Engineering, 2012.

[19] W. Grzesik, *Advanced machining processes of metallic materials: theory, modelling and applications*. Elsevier, 2008.

[20] V. P. Astakhov, "The assessment of cutting tool wear," *Int. J. Mach. Tools Manuf.*, vol. 44, no. 6, pp. 637–647, May 2004.

[21] J. A. Olortegui-Yume and P. Y. Kwon, "Tool wear mechanisms in machining," *Int. J. Mach. Mach. Mater.*, vol. 2, no. 3, pp. 316–334, 2007.

[22] A. Nordgren, B. Z. Samani, and R. M. Saoubi, "Experimental Study and Modelling of Plastic Deformation of Cemented Carbide Tools in Turning," *Procedia CIRP*, vol. 14, pp. 599–604, 2014.

[23] P. K. Wright and E. M. Trent, *Metal Cutting*, 4th ed. Woburn: Butterworth-Heinemann, 2000.

[24] B. M. Kramer, "Tribological Aspects of Metal Cutting," *J. Eng. Ind.*, vol. 115, pp. 372–376, 1993.

[25] I. M. Hutchings and P. Shipway, *Tribology: friction and wear of engineering materials*, 2nd ed. Butterworth-Heinemann, 2017.

[26] American Society for Testing and Materials, "ASTM G40-17: Wear and Erosion," *Annu. B. ASTM Stand.*, vol. i, pp. 1–9, 2017.

[27] E. Rabinowicz, *Friction and Wear of Materials*. 1965.

[28] B. M. Kramer and P. K. Judd, "Computational design of wear coatings," *J. Vac. Sci. Technol. A Vacuum, Surfaces, Film.*, vol. 3, no. 6, p. 2439, 1985.

[29] S. Ramalingam and P. K. Wright, "Abrasive Wear in Machining: Experiments With Materials of Controlled Microstructure," *J. Eng. Mater. Technol.*, vol. 103, no. 2, p. 151, Apr. 1981.

[30] F. Halila, C. Czarnota, and M. Nouari, "Analytical stochastic modeling and experimental investigation on abrasive wear when turning difficult to cut materials," *Wear*, vol. 302, no. 1–2, pp. 1145–1157, 2013.

[31] M. Binder, F. Klocke, and B. Doebbeler, "Abrasive wear behavior under metal cutting conditions," *Wear*, vol. 376–377, pp. 165–171, Apr. 2017.

[32] T. Wong, W. Kim, and P. Kwon, "Experimental support for a model-based prediction of tool wear," *Wear*, vol. 257, no. 7–8, pp. 790–798, 2004.

[33] B. M. Kramer and N. P. Suh, "Tool Wear by Solution: A Quantitative Understanding," *J. Eng. Ind.*, vol. 102, no. 4, pp. 303–309, 1980.

[34] B. M. Kramer, "Predicted wear resistances of binary carbide coatings," *J. Vac. Sci. Technol. A Vacuum, Surfaces, Film.*, vol. 4, no. 6, pp. 2870–2873, 1986.

[35] J. A. Olortegui-Yume and P. Y. Kwon, "Local Crater Wear Prediction Using Physics-Based Models," *J. Manuf. Sci. Eng.*, vol. 132, no. 5, p. 051007, 2010.

[36] P. D. Hartung, B. M. Kramer, and B. F. von Turkovich, "Tool Wear in Titanium Machining," *CIRP Ann. - Manuf. Technol.*, vol. 31, no. 1, pp. 75–80, 1982.

[37] S. Odelros, B. Kaplan, M. Kritikos, M. Johansson, and S. Norgren, "Experimental and theoretical study of the microscopic crater wear mechanism in titanium machining," *Wear*, vol. 376–377, pp. 115–124, 2017.

[38] D. Mari, "Mechanical Behavior of Hardmetals at High Temperature," in *Comprehensive Hard Materials*, vol. 1, Elsevier Ltd, 2014, pp. 405–421.

[39] G. Östberg and H.-O. Andrén, "Microstructural changes during wear by plastic deformation of cemented carbide and cermet cutting inserts," *Metall. Mater. Trans. A*, vol. 37, no. 5, pp. 1495–1506, 2006.

[40] T. Aiso, U. Wiklund, M. Kubota, and S. Jacobson, "Effect of Si and Al additions to carbon steel on material transfer in turning with CVD coated tools," *Wear*, vol. 97, no. 368–369, pp. 379–389, 2016.

[41] V. Bushlya, F. Lenrick, J. E. Ståhl, and R. M'Saoubi, "Influence of oxygen on the tool wear in machining," *CIRP Ann.*, 2018.

[42] J. C. Hamann, F. Meslin, and J. Sartkulvanich, "Criteria for the quality assessment of constitutive equations dedicated to cutting models," *Mach. Sci. Technol.*, vol. 6, no. 3, pp. 331–351, 2002.

[43] S. Olovsjö, a. Wretland, and G. Sjöberg, "The effect of grain size and hardness of wrought Alloy 718 on the wear of cemented carbide tools," *Wear*, vol. 268, no. 9–10, pp. 1045–1052, Mar. 2010.

[44] S. Cedergren, S. Olovsjö, G. Sjöberg, and L. Nyborg, "The effects of grain size and feed rate on notch wear and burr formation in wrought Alloy 718," *Int. J. Adv. Manuf. Technol.*, vol. 67, no. 5–8, pp. 1501–1507, Jul. 2013.

[45] S. Olovsjö, A. Wretland, and G. Sjöberg, "The effect of grain size and hardness of Waspaloy on the wear of cemented carbide tools," *Int. J. Adv. Manuf. Technol.*, vol. 50, no. 9–12, pp. 907–915, 2010.

[46] L. Jiang, Å. Roos, and P. Liu, "The influence of austenite grain size and its distribution on chip deformation and tool life during machining of AISI 304L," *Metall. Mater. Trans. A*, vol. 28, no. 11, pp. 2415–2422, 1997.

[47] J. Angseryd, E. Olsson, and H.-O. Andrén, "Effect of workpiece sulphur content on the degradation of a PCBN tool material," *Int. J. Refract. Met. Hard Mater.*, vol. 29, no. 6, pp. 674–680, Nov. 2011.

[48] N. Ånmark and T. Björk, "Effects of the composition of Ca-rich inclusions on tool wear mechanisms during the hard-turning of steels for transmission components," *Wear*, vol. 368–369, pp. 173–182, 2016.

[49] N. Ånmark, S. Lövquist, M. Vosough, and T. Björk, "The Effect of Cleanliness and Micro Hardness on the Machinability of Carburizing Steel Grades Suitable for Automotive Applications," *Steel Res. Int.*, vol. 87, no. 4, pp. 403–412, 2016.

[50] N. Ånmark, A. Karasev, and P. G. Jönsson, "The effect of different non-metallic inclusions on the machinability of steels," *Materials (Basel).*, vol. 8, no. 2, pp. 751–783, 2015.

[51] O. Bletton, R. Duet, and P. Pedarre, "Influence of oxide nature on the machinability of 316L stainless steels," *Wear*, vol. 139, no. 2, pp. 179–193, 1990.

[52] "CES EduPack." Granta Design Limited, 2019.

[53] G. Krauss, *Steels - Processing, Structure, and Performance*. ASM International, 2005.

[54] Uddeholms AB, "VANADIS ® 10 SUPERCLEAN."

[55] A. Malakizadi, H. Gruber, I. Sadik, and L. Nyborg, "An FEM-based approach for tool wear estimation in machining," *Wear*, vol. 368–369, pp. 10–24, 2016.

[56] K. B. Surreddi, K. Björkeborn, and U. Klement, "Effect of Heat Treatment on Chip Formation in a Case Hardening Steel," *J. Mater. Chem. Eng.*, vol. 1, no. 1, pp. 1–7, 2013.

[57] R. E. Schafrik and R. Sprague, "Saga of gas turbine materials, part III," *Adv. Mater. Process.*, vol. 162, no. 5, pp. 29–33, 2004.

[58] C. T. Sims, N. S. Stoloff, and W. C. Hagel, *Superalloys II*, 2nd ed. New York: Wiley-Interscience, 1987.

[59] J. I. Goldstein *et al.*, *Scanning Electron Microscopy and X-ray Microanalysis*. Boston, MA: Springer US, 2003.

[60] Oxford Instruments, "HKL Channel 5 EBSD post-processing software." 2011.

[61] S. I. Wright, M. M. Nowell, and D. P. Field, "A Review of Strain Analysis Using Electron Backscatter Diffraction," *Microsc. Microanal.*, vol. 17, pp. 316–329, 2011.

[62] M. A. Meyers and K. K. Chawla, *Mechanical Behavior of Materials*, vol. 2008. Cambridge University Press, 2008.

[63] ASTM International, "ASTM E112-13 Standard Test Methods for Determining Average Grain Size," West Conshohocken, PA, 2013.

[64] W. Rasband, "ImageJ." National Institutes of health, USA, 2018.

[65] M. Matula *et al.*, "Intergranular corrosion of AISI 316L steel," *Mater. Charact.*, vol. 46, no. 2–3, pp. 203–210, Feb. 2001.

[66] S. Olovsjö and L. Nyborg, "Influence of microstructure on wear behaviour of uncoated WC tools in turning of Alloy 718 and Waspaloy," *Wear*, vol. 282–283, pp. 12–21, Apr. 2012.

[67] R. Polvorosa, A. Suárez, L. N. L. de Lacalle, I. Cerrillo, A. Wretland, and F. Veiga, "Tool wear on nickel alloys with different coolant pressures: Comparison of Alloy 718 and Waspaloy," *J. Manuf. Process.*, vol. 26, pp. 44–56, 2017.

[68] A. Kagawa, T. Okamoto, K. Saito, and M. Ohta, "Hot hardness of (Fe, Cr) 3 C and (Fe, Cr) 7 C 3 carbides," *J. Mater. Sci.*, vol. 19, no. 8, pp. 2546–2554, 1984.

[69] J. H. Westbrook and E. R. Stover, "Carbides for high-temperature applications," *Pap. From High-Temperature Mater. Technol.*, pp. 312–348, 1967.

[70] D. L. Kohlstedt, "The temperature dependence of micro- hardness of the transition-metal carbides," *J. Mater. Sci.*, vol. 8, pp. 777–786, 1973.

[71] A. Kagawa and T. Okamoto, "Hot hardness of cementite," *J. Mater. Sci.*, vol. 18, no. 1, pp. 225–230, 1983.

[72] H. C. Chao, L. H. Van Vlack, F. Oberlin, and L. Thomassen, "Inclusion deformation: II: Hardness of MnS-FeS microstructures.," 1962.

[73] J. Lankford, "Comparative study of the temperature dependence of hardness and compressive strength in ceramics," *J. Mater. Sci.*, vol. 18, no. 6, pp. 1666–1674, 1983.

[74] R. Koester and D. Moak, "Hot Hardness of Selected Borides , Oxides , and Carbides to 19OO C," *J. Am. Ceram. Soc.*, vol. 60, no. 6, pp. 290–296, 1967.

[75] A. Miyoshi and A. Hara, "High Temperature Hardness of WC , TiC , TaC , NbC and Their

Mixed Carbides," *J. Japan Soc. Powder Metall.*, vol. 12, no. 2, pp. 78–84, 1965.

[76] A. G. Atkins and D. Tabor, "Hardness and Deformation Properties of Solids at Very High Temperatures," *Proc. R. Soc. A Math. Phys. Eng. Sci.*, vol. 292, no. 1431, pp. 441–459, Jun. 1966.

[77] J. J. Oakes, "A comparative evaluation of HfN, Al2O3, TiC and TiN coatings on cemented carbide tools," *Thin Solid Films*, vol. 107, no. 2, pp. 159–165, 1983.

[78] P. C. Jindal, A. T. Santhanam, U. Schleinkofer, and A. F. Shuster, "Performance of PVD TiN, TiCN, and TiAlN coated cemented carbide tools in turning," *Int. J. Refract. Met. Hard Mater.*, vol. 17, no. 1, pp. 163–170, 1999.

[79] M. S. Koval'chenko, V. V. Dzhemelinskii, V. N. Skuratovskii, Y. G. Tkachenko, D. Z. Yurchenko, and V. I. Alekseev, "Microhardness of some carbides at various temperatures," *Sov. Powder Metall. Met. Ceram.*, vol. 10, no. 8, pp. 665–668, 1971.

[80] V. N. Skuratovskii, Y. G. Tkachenko, and V. A. Borisenko, "A technique for investigating the microhardness of refractory compounds within a wide temperature range," *Strength Mater.*, vol. 1, no. 4, pp. 393–396, Oct. 1969.

[81] M. Lee, "High temperature hardness of tungsten carbide," *Metall. Trans. A*, vol. 14, no. 8, pp. 1625–1629, 1983.

[82] P. Hoier, A. Malakizadi, U. Klement, and P. Krajnik, "Characterization of abrasion- and dissolution-induced tool wear in machining," *Wear*, vol. 426–427, pp. 1548–1562, 2019.

[83] J. Davies, *ASM Speciality Handbook: Heat Resistant Materials*. ASM International, 1997.

[84] High Temp Metals, "WASPALOY TECHNICAL DATA." [Online]. Available: https://www.hightempmetals.com/techdata/hitempWaspaloydata.php. [Accessed: 10-Jul-2019].

[85] P. Hoier, A. Malakizadi, P. Stuppa, S. Cedergren, and U. Klement, "Microstructural characteristics of Alloy 718 and Waspaloy and their influence on flank wear during turning," *Wear*, vol. 400–401, pp. 184–193, Apr. 2018.

[86] A. Nordgren and A. Melander, "Tool wear and inclusion behaviour during turning of a calcium-treated quenched and tempered steel using coated cemented carbide tools," *Wear*, vol. 139, no. 2, pp. 209–223, 1990.

[87] R. Kiessling and N. Lange, *Non-metallic inclusions in steel*. London: The Iron and Steel Institute, 1964.

[88] R. Kiessling and N. Lange, *Non-metallic inclusions in steel (Part II)*. London: The Iron and Steel Institute, 1966.

[89] R. Kiessling, *Non-metallic inclusions in steel (Part V)*. London: The Institute of Metals, 1989.

[90] R. Kiessling, *Non-metallic inclusions in steel (Part III)*. London: The Iron and Steel Institute, 1968.

[91] P. Hoier, A. Malakizadi, S. Friebe, U. Klement, and P. Krajnik, "Microstructural variations in 316L austenitic stainless steel and their influence on tool wear in machining," *Wear*, Feb. 2019.